EFFECT OF PORE PRESSURE DEPLETION ON WELLBORE STABILITY AND HYDRAULIC FRACTURING IN SANDSTONE RESERVOIR

BY

MOHAMMED JABER AL DOSSARY

A Thesis Presented to the

DEANSHIP OF GRADUATE STUDIES

KING FAHD UNIVERSITY OF PETROLEUM & MINERALS

DHAHRAN, SAUDI ARABIA

In Partial Fulfillment of the
Requirements for the Degree of
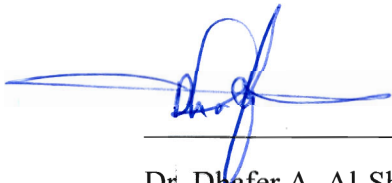
MASTER OF SCIENCE

In

PETROLEUM ENGINEERING

DECEMBER 2018

KING FAHD UNIVERSITY OF PETROLEUM & MINERALS

DHAHRAN- 31261, SAUDI ARABIA

DEANSHIP OF GRADUATE STUDIES

This thesis, written by **Mohammed Jaber Al Dossary** under the direction of his thesis advisor and approved by his thesis committee, has been presented and accepted by the Dean of Graduate Studies, in partial fulfillment of the requirements for the degree of **MASTER OF SCIENCE IN PETROLEUM ENGINEERING.**
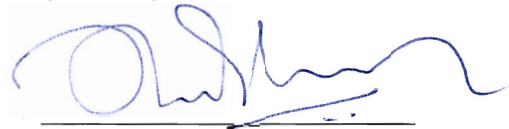
Dr. Dhafer A. Al-Shehri
Department Chairman

Dr. Salam A. Zummo
Dean of Graduate Studies

10/ 12/ 2018
Date

Dr. Salaheldin Elkatatny
(Advisor)

Dr. Abdulazeez Abdulraheem
(Member)

Dr. Mohamed Mahmoud
(Member)

Dedication

This thesis work is dedicated to my family, whom have been always a constant source of support and encouragement during the challenges of graduate school and life. I am truly thankful for having them in my life. This work is also dedicated to my father, who passed away last year. He gone forever away from our loving eyes and who left a void never to be filled in our lives.

Mohammed

ACKNOWLEDGMENTS

First of all, I would like to thank my thesis advisor Dr. Salaheldin Elkatatny. The door of Dr. Elkatatny office was always open whenever I have a question about my Thesis.

I would also like to acknowledge Mr. Osman Hamid, Saudi Aramco. I am grateful to him for his guidance and very valuable comments on this thesis. He consistently allowed this paper to be my own work but steered me in the right the direction whenever he thought I needed it.

I would also like to thank the thesis committee who were involved in reviewing the input and output for this research project. Without their passionate participation and input, the thesis could not have been successfully submitted.

Finally, I would like to express my deep gratitude to my family for providing me with constant support and continuous encouragement throughout my years of study and through the process of researching and writing this thesis. This accomplishment would not have been possible without them. Thank you.

Author

[Mohammed Al-Dossary]

TABLE OF CONTENTS

LIST OF TABLES

LIST OF FIGURES

ABSTRACT

Full Name   : [Mohammed Jaber Al-Dossary]

Thesis Title   : [Effect of Pore Pressure Depletion on Wellbore Stability and Hydraulic Fracturing in Sandstone Reservoir]

Major Field   : [Master of Science in Petroleum Engineering]

Date of Degree : [October 2018]

Development of various challenging reservoirs with severe stress sensitivity is raising awareness that geomechanics is a vital aspect of reservoir management. Understanding reservoir geomechanical behavior is becoming more and more important for petroleum industry. A significant change in formation pressure caused by either injection/depletion will induce deformation and stress/strain changes in the reservoir, understanding of in-situ stresses and how stress changes with reservoir injection/depletion and pore pressure increase or drawdown is important in a multidisciplinary approach to reservoir characterization and management.

These changes in stresses/strain affect the reservoir as well as the overburden layers and directly affect all of the operations, such as drilling, stimulation and production strategies. Stress affects nearly all petrophysical properties. Reservoir compaction, shear casing and well damage, cap-rock integrity, fault reactivation and sand production can occur during reservoir depletion.

To address these issues, development of 3D geomechanical models (which describe the state of stresses in the reservoir and overburden) and 4D geomechanics models (dynamic models, that describe the changes in stress over time with either production or injection) are required.

Reservoir Geomechanics approaches, presented in this thesis address and answer the following questions:

1. How Geomechanics changes in stresses and strain impact wellbore stability related issues and stimulation operations?

2. Stress rotation around faulted zones.

3. How depletion effect hydraulic fracture growth?

ملخص الرسالة

الاسم الكامل: محمد جبر الدوسري

عنوان الرسالة: تأثيرضغط المسام على ثبات حفرة البئر والتكسير الهيدروليكي في المكامن الرملية

التخصص: هندسة بترول

تاريخ الدرجة العلمية:

إن تطوير العديد من المكامن الصعبة ذات التأثر الشديد بالضغط يؤدي الى زيادة الوعي بأن الجيولوجيا الميكانيكة هي جانب حيوي في إدارة المكامن. إن فهم السلوك الجيوميكانيكي للمكمن أصبح أكثر وأكثر أهمية بالنسبة للصناعه البترولية. التغير الكبير للضغط الناجم عن الاستنزاف بسبب الانتاج يؤدي إلى حدوث التشوه,الإجهاد والانفعال في المكمن، وفهم الإجهادات وكيفية تغير الإجهاد مع استنزاف الخزان وزيادة أو نقص ضغط المسام أمر مهم بعدة طرق او توجهات لتوصيف وادارة المكمن.

تؤثر هذه التغيرات في الإجهاد / الإنفعال على الخزان وكذلك الطبقات المفرطة بالضغط وتؤثر بشكل مباشر على جميع العمليات ، مثل استراتيجيات الحفر والتحفيز والإنتاج. الإجهاد يؤثر على جميع خصائص البتروفيزيائية تقريبا.

يمكن أن يحدث انضغاط المكمن (تصبح طبقاته مرصوصة) وضرر في البئر وجدرانه واحتمالية كبس الصخور وإعادة تنشيط التصدعات في الارض وإنتاج الرمال أثناء الانتاج من المكمن. لمعالجة هذه القضايا ، تطوير نماذج جيوميكانيكية ثلاثية الأبعاد (التي تصف حالة الإجهاد في الخزان والعبء الزائد) ونماذج جيوميكانيكية رباعية الأبعاد (النماذج الديناميكية ، التي تصف التغيرات في الإجهاد بمرور الوقت مع الإنتاج أو الحقن) تكون مطلوبة.

نهج الخزان الجيوميكانيكي ، قدم في هذه الرسالة للإجابة على الأسئلة التالية:

- كيف تتغير الجيولوجيا الميكانيكية في الضغوط والإجهاد وتأثيرها على ثبات حفرة البئر والمشاكله المتعلقة بها وعمليات التنشيط؟
- دوران الإجهاد حول المناطق المتصدعة.
- كيف يؤثر النفاد على نمو الكسر الهيدروليكي؟

CHAPTER 1

INTRODUCTION

1.1   Introduction

Development of various challenging reservoirs with severe stress sensitivity is raising awareness that Geomechanics is a vital aspect of reservoir management. Understanding the reservoir geomechanical behavior becomes more and more important for the petroleum industry.

A 3D geomechanical model will be developed for a sector of sandstone gas reservoir in Saudi Arabia. Properties from the 3D model were used to populate a finite element model to determine changes in stresses and strain as reservoir pressure decreased due to production.

The induced changes in stresses, strains and displacement patterns will be modeled using different depletion rates and pressure to ensure the integrity of the reservoir rock and surrounding formation.

The research also study the effects of the changes on the surrounding formation to determine the critical pressure changes that effect cap-rock integrity, fault re-activation and tensile failure.

The efficiency of hydraulic fractures depends mainly on reservoir and completion quality parameters. Geomechanical characterization of the magnitude and orientation of in-situ stresses and mechanical properties play a major role in understanding the growth and behavior of hydraulic fractures.

A 3D methodology for pore pressure prediction based on seismic data has been extensively documented by Dutta (2002). Sayers et al. (2002) and Dutta and Khazanehdari (2006). All seismic velocity-based pore pressure prediction methods rely on the premise that seismic velocity is sensitive to effective stress and overpressure. This premise generally holds true for cases of young sediments with fast deposition. For these sediments, under-compression is the main overpressure mechanism for which seismic velocity is sensitive to effective stress and then overpressure, Qui (2013).

1.2   Problem Statement and Research Objective

• Many operations in oil and gas industry require a coupling between geomechanics and fluid flow to understand the effect of changes in reservoir pressure.

• Wellbore stability related issues will be experienced while drilling depleted zones due changes in the mud weight window, loss of circulations and wellbore collapse might be occurred in the same zones.

• Hydraulic fracture might grow into a depleted zone if there is strong barrier.

• Stress rotation around faulted and fractured areas due to depletion.

The objectives of this research are to characterize; stresses, strain and rock failure due to changes in pore pressure resulting from reservoir injection/depletion. Moreover, the answers of the below statement will be captured:

1. How Geomechanics changes in stresses and strain impact wellbore stability related issues and stimulation operations

2. Stress rotation around faulted zones

3. How depletion effect hydraulic fracture growth

CHAPTER 2

LITERATURE REVIEW

2.1   Building a Reservoir Geomechanical model

2.1.1   General

The needed data that is used for the purpose of conducting a geomechanical modeling including in-situ stresses characterization by pore pressure prediction and depletion effect on hydraulic fracturing should start initially by gathering all the available information to help generates the most valuable model. Usually the required information is the location map to know the studied area boundary, log data for the off-set wells, seismic data and faults, velocity model, global density model and vertical stress model which is already documents by Qui 2013. Further description will be on next sections.

2.1.2   1D Geomechanical Model (GM)

Mechanical Earth Model (MEM) typically includes elastic properties, rock strength, pore pressure, and the in-situ stress magnitudes and directions. It is usually generated by combining log measurements with laboratory test results on core samples and with other measurements and information acquired during drilling and well construction. Mechanical earth model is a numerical representation of the state of stress and rock mechanical properties for precise stratigraphic section in field or reservoir (Plumb et al 2000).

A calibrated MEM contains information that can be used in drilling and stimulation operation such as stress orientation for planning a horizontal well and its completion. Moreover, an MEM contains all available information required to assess how rocks and fractures deform in response to drilling, completion and production operations (Thomas Berad et al 2016).

Yuezhi (1997) has developed a model for in-situ stresses characterization in anisotropic formations. He started with mechanical earth modeling and then calibrate the model using core testing data.

Owing to rock having different degrees of anisotropy, it is more comprehansive to consider formation rocks as transversely isotropic material than by previous methods, value of in-situ stresses are closer to practical values.

The key to detrmine elastic parameters in transversely isotropic material in lab is to detrmine formation and direction dip, relative to core orientation. Although the method to detarmine elastic parameters of rock in lab is accurate, it is imposible to acquire continuous cross sections due to limit of quantity of cores.

2.1.3 3D Geomechanical Model

In 2013, Qui et al established a workflow for 3D reservoir geomechanics for tight reservoir. The workflow of Building a 3D geomechanical model in sandstone formation as illustrated in Fig.1 starts with analyzing and calibrating well log data and core data to generate a calibrated 1D geomechanical model a detailed workflow .
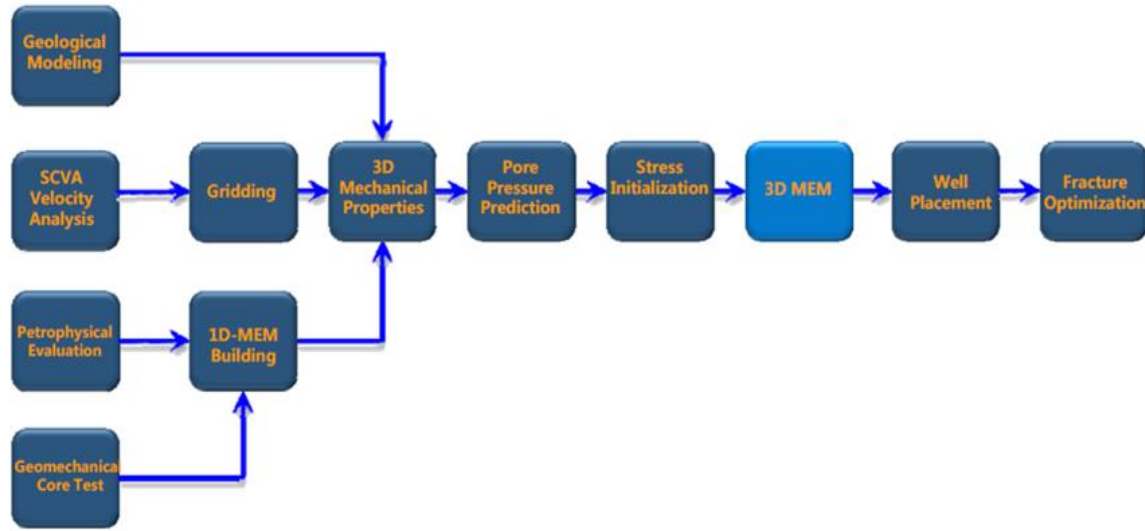
Figure 1 The workflow of 3D reservoir geomechanics for tight reservoirs, (Qui 2013)

Hamid et al (2015) conducted 3D geomechanics simulation, which was investigated the effects of depletion in complex tight carbonate gas reservoir. The magnitude of σ_H decreases in the depleted area but the adjoining layers experience higher σ_H. This change in stress increases the stress contrast between the layers. The case study shows that the higher stress can act as stress barrier and stop the propagation of hydraulic fractures. The stress contrast in adjoining layers due to depletion cannot be estimated using 1D geomechanical models. A 3D geomechanical model is helpful tool in designing hydraulic fractures in complex depleted tight reservoirs.

2.1.4 4D Geomechanical Model

The use of time-lapse seismic (4D) surveys for monitoring producing oil and gas fields has become widespread in oil and gas industry. Many types of physical changes can be detected with time-lapse seismic surveys and published examples include observing effects due to fluid movements (e.g. Koster et al. 2000) as well as pressure depletion (e.g. Guilbot and

Smith, 2002). In a depleted reservoir, there are several mechanisms that produce potentially observable 4D effects (Herwanger et al 2011). There are changes that occur within the reservoir unit such as:

• Compaction effects due to the change in the effective stress field.

• Changes in compressional (v_p) and shear (v_s) velocities as a result of compaction.

• Changes in the pore-fill properties that depend on pressure.

There are also changes that occur in the rocks bounding the reservoir. The subsidence that occurs from reservoir compaction is not uniformly distributed above the reservoir because of rock mechanical constraints. The compacting reservoir produces long-wavelength changes in the stress (and strain) tensor of the bounding rocks that are spatially variable. These stress-field changes in the non-reservoir rocks can reveal themselves on our time-lapse seismic as differences in arrival times and possibly as changes in reflection strength , Dusselt.

Time-lapse (4D) seismic monitoring of pressure-induced changes in depleting gas fields reveals that detectable differences in seismic arrival times are observed above the reservoir interval. Geomechanical models of depleting reservoirs predict that because of reservoir compaction due to pressure depletion, changes in the long-wavelength stress and strain fields occur in the rocks bounding the reservoir. Models incorporating the geomechanical stress and strain field changes predict changes in the two-way arrival times that are compared with actual time-shift observations at a depleting gas field in the North Sea, Herwanger. The geomechanical-based predictions are in good agreement with the

observations. Detecting geomechanical changes in the over- and underburden rocks opens up new ways of using 4D data, especially in places where the signal from the reservoir rocks is small.

2.1.5 Coupled Reservoir and geomechanical modeling

2.1.5.1 Levels of coupling

There are different levels of coupling between fluid-flow and geomechanics processes, some of which are described and summarized below by Jalali & Dusseault, 2008 and P. Longuemare et al, 2002 :

Decoupled method

This method is the loosest coupling technique among coupling methods. In this case, the effect of stress changes is introduced to the flow model via some parameters such as compressibility and permeability. After flow simulation, deformation is calculated in a geomechanical model in which pressure history is applied as an external load. This process is then repeated until a suitable estimation for pressure and temperature is achieved.

Pseudo coupling

This method of coupling is based on an empirical model of absolute permeability and porosity as functions of pressure. During this process, a conventional reservoir simulator computes some geomechanical parameters such as compaction (via relationships between porosity and vertical displacement) and horizontal stress changes (using relationships between porosity and stress). Usually, the empirical model is a table of porosity and

absolute permeability versus pressure which is then introduced to the simulator. The permeability may then be altered for the next time-step in the numerical simulation. This method is not very realistic, but may be applied in cases where the computational costs for fully coupled modeling are prohibitive.

Explicit coupling

In this approach, which is also called the one-way coupling method, information from a reservoir simulator is sent to a geomechanics model, but results from the geomechanics calculations are not fed back to the reservoir simulator. In this case, the reservoir fluid flow is not affected by geomechanical responses calculated by the geomechanics module.

However, change in reservoir flow variables will affect the geomechanics variables. This coupling is an efficient and time-saving approach for subsidence problems because geomechanical calculations can be performed on a different time scale than fluid-flow calculations. Fluid-flow usually propagates in a short time-step frame within flow simulation, in comparison with deformation (subsidence) calculation, which can be done when needed.

So, by using different time scales for flow and geomechanical simulation, performance of the simulation will be enhanced. This method is a flexible and straightforward technique for coupling that can use an existing flow/ geomechanics simulators, simultaneously.

On the other hand, one of the big concerns in this technique is its stability and accuracy that imposes some time-step restrictions on runs. However, for most of subsidence issues,

time steps is needed for fluid-flow calculations that should be less than those imposed by the explicit coupling calculations.

Iterative coupling

In this coupling method, which is also known as two-way coupling, information computed in reservoir simulator and geomechanics model is exchanged back-and-forth through nonlinear iterations for each time-step. Therefore, reservoir flow is affected by geomechanical responses as calculated by the geomechanics model.

A simulator performs computations sequentially for a multiphase porous flow and displacements during each nonlinear iteration. Flow and displacement calculations are coupled through calculations of pore volumes (or reservoir porosity) at the end of each nonlinear iteration. The main advantage of this coupling is its flexibility, i.e., the two systems can be solved by different numerical methods. In addition, a conventional reservoir simulator can be coupled with a suitable geomechanics module with modest modifications in both codes.

This method will be challenging for difficult problems as it may require a large number of iterations due to a first-order convergence rate in the nonlinear iterations. Another bottleneck to this technique is that only relatively small jumps in pore volume (or the reservoir porosity) can be handled due to the large volume of fluids which must move to the wells to conserve mass when compaction occurs in the field.

An iteratively coupled approach will produce the same results as a fully coupled approach if both techniques use sufficiently tight convergence tolerances for iterations.

Full coupling

In this approach, fluid-flow and displacement calculations are performed together using one discretization system, which is usually the finite element method, and one of the program's linear solver function is to handle both fluid-flow/ displacement variables simultaneously. The primary attraction of the fully coupled approach is that it is the most stable approach of all the techniques and it preserves second-order convergence of nonlinear iterations. The solution is reliable and can be used as a benchmark for other coupling approaches.

Drawbacks to the fully coupled approach include the following: it may be difficult to couple existing porous-flow simulators and geomechanics simulators, it requires more code development than other techniques, and it can be slower than the explicit and iterative techniques used on some problems. However, this approach is the "gold standard" of numerical coupling methods.

2.1.5.2 Coupling methods

According to Settari and Mourits (1998), there are two main components of the coupling between fluid-flow and geomechanics.

Volume coupling

Pore volume changes as a result of stress, pressure or temperature variations are considered in this case. For convergence purpose, the calculated pore volume changes should be equal in both fluid flow and geomechanics models. The pore volume changes from the

geomechanics model are usually more accurate than those of the fluid flow model because it is computed by volumetric strain through a complex and hopefully more realistic material constitutive model than simple constant pore compressibility. This coupling is more suitable for problems, which deal with large porosity changes resulting from shear or plastic deformation. These problems are common in unconsolidated heavy oils, soft compacting reservoirs, oil sands, North Sea chalk, California diatomite and perhaps some other materials such as coal.

Coupling through flow properties

In this approach to coupling, changes in permeability and relative permeability are related to changes in stress, shear stress, or compaction. When shear occurs in a porous medium, the nature of the medium is changed, leading to an alteration in permeability and relative permeability. This is important in reservoirs where compressibility effects do not have a significant role in the volumetric behavior, such as gas reservoirs in which volume coupling is not important. Another example is a water-flooding process with an injection pressure close to or above fracturing pressure, generating enhancement in the permeability around injectors or induced fracture zones (e.g. by shear dilation).

2.2   In-situ Stresses

In sedimentary basins with relatively flat-lying rock strata and limited ground surface relief, it is reasonable to assume that the vertical stress at any point within these strata is due simply to the weight of the overburden. Further, there are no shear stresses acting in the vertical direction in such a setting, hence the vertical stress is a principal stress component. Due to the orthogonal nature of principal stresses, the other two principal

stresses lie in the horizontal plane, and are oriented at right angles to one another. As such, the in-situ stress state at any point may be fully defined by specifying the magnitudes of the vertical stress (σ_v), the maximum horizontal stress (σ_{Hmax}) and the minimum horizontal stress (σ_{Hmin}), as well as the orientation of either one of the horizontal stresses. These stress components are illustrated in **Fig.2.** (Hamid 2008)
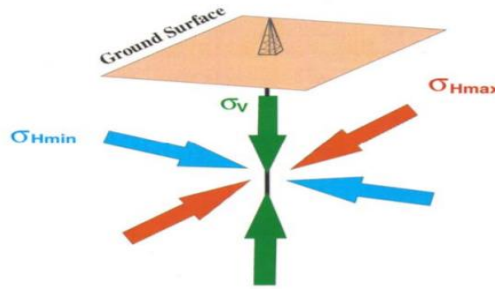
Figure 2 Principal in-situ stress components acting on a point in the subsurface (after Bell et.,1994)

2.2.1 Vertical Stress Magnitude

Subsurface rock units carry the weight of the overlying rocks, sediments and pore fluids. The vertical stress at a given depth, z, results from this weight. The magnitude of this vertical (or "overburden") stress, σ_v can be calculated by integrating bulk density measurements of the overburden as follows:

$$\sigma_v(z) = \int_0^z \rho(z) g \, dz \qquad \textbf{Eq. 1}$$

Where:

σ_v = vertical in-situ stress (MPa)

ρ_b = bulk density (kg/m^3)

z = depth from ground surface (m)

g = acceleration due to gravity (9.81 m/s^2)

In this thesis, as in most petroleum geomechanics studies, bulk density data were available from density logging tools. These tools measure densities at discrete intervals (often approximately 15 cm). Density measurements usually acquired for the reservoir sections, and hence overburden stress calculated from the surface to the depth of interest, the non-reservoir interval density can be estimated using the following correlation (Sayers 2011)

$$\rho = \rho_0 + az^b \qquad \textbf{Eq. 2}$$

2.2.2 Horizontal Stresses

The magnitude of the minimum and maximum horizontal stresses has been calculated using the following correlations, Hamid et al 2018:

$$\sigma_{hmin} = \frac{v}{1-v}\sigma_V + \frac{1-2v}{1-v}\alpha P_p + \frac{E}{1-v^2}\varepsilon_x + \frac{vE}{1-v^2}\varepsilon_y \qquad \textbf{Eq. 3}$$

$$\sigma_{hmax} = \frac{v}{1-v}\sigma_V + \frac{1-2v}{1-v}\alpha P_p + \frac{E}{1-v^2}\varepsilon_y + \frac{vE}{1-v^2}\varepsilon_x \qquad \textbf{Eq. 4}$$

2.3　Pore Pressure Prediction

A 3D methodology for pore pressure Prediction based on seismic data has been extensively documented by Dutta (2002). Sayers et al. (2002) and Dutta and Khazanehdari (2006). All seismic velocity-based pore pressure prediction methods rely on the premise that seismic velocity is sensitive to effective stress and overpressure. This premise generally holds true for cases of young sediments with fast deposition. For these sediments, under-compression

is the main overpressure mechanism for which seismic velocity is sensitive to effective stress and then overpressure.

Pore pressure gradient is a measure of the change in the pressure that applied on the fluids in the spaces between pore of buried rocks as a function of depth. These pressure gradients vary as a function of depositional history, compaction, mineralogy, depth of burial and other environmental conditions. The normally pressure section has a pore pressure gradient equal to that of a water column unimpeded by permeability. It is said that the reservoir is in hydraulic communication with the surface. Sections where the flow of pore fluids is restricted, for any mechanism, are called abnormally pressured or geo-pressured. Abnormally pressured sections can be under-pressured but are more typically over-pressured **Fig. 3**. Additionally, it shows a typical pore pressure measurement bounded by the hydrostatic gradient to the left and the lithostatic gradient to the right. (Although represented by straight lines in this cartoon, the actual values for the bounding lines are modified by salinity, temperature and mineralogy.) (Lindsay et., 1997)
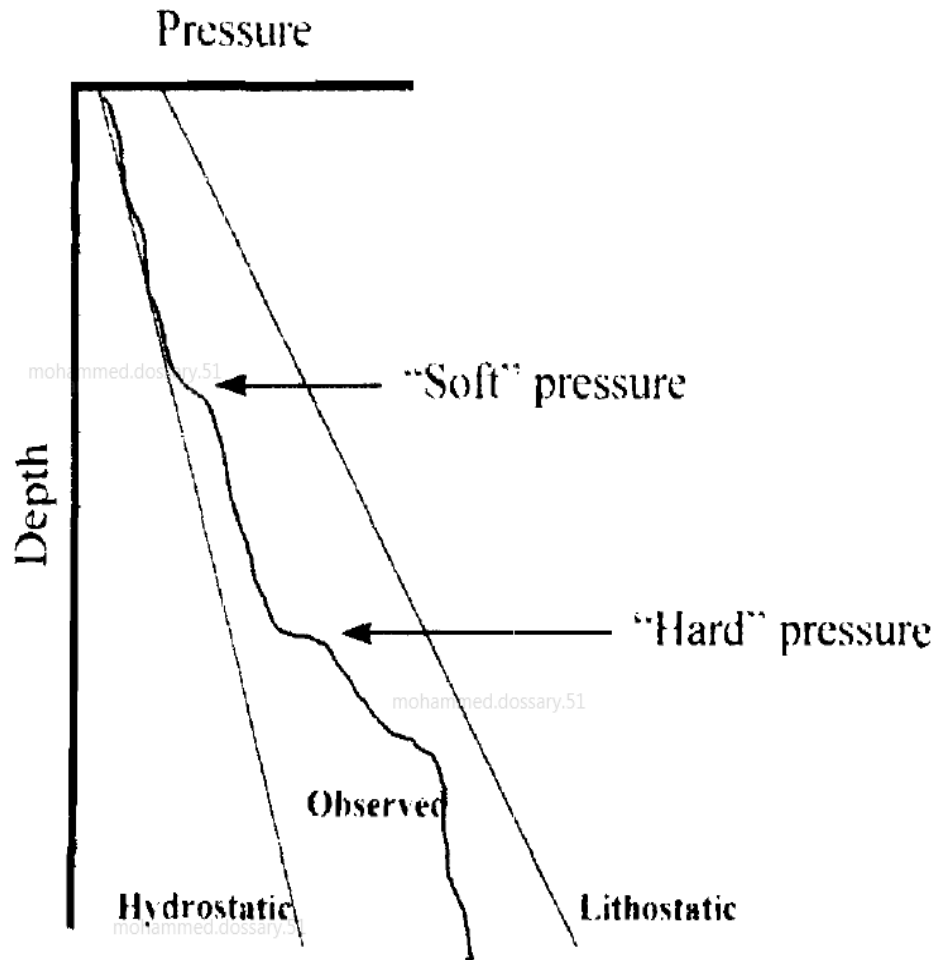
Figure 3   Typical pore pressure measurement (Lindsay et., 1997)

In 1997, Lindsay developed a three-dimension pore pressure prediction from seismic interval velocity. The empirical relationship between seismic interval velocity and pore pressure gradient is exploited for the prediction of pore pressure gradients in areas where direct measurements are impractical. These velocities are the ouput of seismic trace data processing for normal-move-out (NMO) correction, dip-move-out (DMO) correction and the event migration for correct structural imaging. Seismic migration velocities are a precise measure of a specific average velocity type called RMS

velocities (for Root Mean Squared velocities). From RMS velocity. Interval velocity is calculated.

Rock Property and Reflectivity Modeling: The primary tool for rock properties modeling is the Biot-Gassmann-Gertzma equations4. These equations collectively referred to as the Gassmann equations, represent models of solid and fluid behavior in the presence of the stresses associated with seismic wave propagation. The models are surprisingly precise in light of the assumptions associated with their use. Many times the averaging effects of the seismic wavelet benefit the geoscientist. The most significant and most violated assumption associated with the Gassmann equations if that the rock-fluid system is a heterogeneous, isotropic, linearly elastic system.

2.4   Mechanical Properties Determination (Dynamic and Static)

Mechanical properties influence the stress and strain distribution in the subsurface. For example, stiff layers concentrate the stresses and soft layers concentrate the strain values. Strength properties will determine whether rock will fail at a given stress or not (Herwanger and Koutsabeloulis 2011). The calculation of the magnitude of the mechanical properties is therefore a key step in building geomechanical models (Hamid 2015).

The majority of laboratory-measured data collected were static measurements (i.e. static E instead of dynamic E). A limited number of dynamic measurement data (i.e. velocity measurements) were available in some source.

Chang et.al. 2006 mentioned that nearly all proposed formulae for determination of rock strength from geophysical logs utilize one (or more) of the following parameters:

• P-wave velocity (v_p), or equivalently, interval transit time ($\Delta t = v_p^{-1}$), which is directly measured,

• Young's modulus (E), which is derived from velocity and density measurements, or

• Porosity (ϕ), which is usually derived from density measurements assuming rock matrix and fluid densities.

Eqs. (5)–(15) in **Table 1** present a number of relationships in common practice (both published and proprietary) for estimating the unconfined compressive strength of sandstones from geophysical logging data. These relations were derived for case studies carried out for markedly different rocks in markedly different geological settings, around the world and compiled in Chang et.al. 2006.

Table 1 Relationships in common practice for estimating the unconfined compressive strength of sandstones z geophysical logging

Eq. no.	UCS (MPa)	Region where developed	General comments	Reference
(5)	$0.035V_p - 31.5$	Thuringia, Germany	–	Freyburg (1972)
(6)	$1200\exp(-0.036\Delta t)$	Bowen Basin, Australia	Fine grained, both consolidatedand unconsolidated sandstones with all porosity range	McNally (1987)
(7)	$1.4138 \times 10^7 \Delta t^{-3}$	Gulf Coast	Weak and unconsolidated	
(8)	$3.3 \times 10^{-20} \rho^2 V_p^4 [(1+\nu) / (1-\nu)]^2 (1-2\nu)$ $[1+0.78V_{clay}]$	Gulf Coast	Applicable to sandstones UCS>30 MPa	Fjaer et al. (1992)
(9)	$1.745 \times 10^{-9} \rho V_p^2 - 21$	Cook Inlet, Alaska	Coarse grained sandstones and conglomerates	Moos et al. (1999)
(10)	$42.1\exp(1.9 \times 10^{-11} \rho V_p^2$	Australia	Consolidated sandstones with $0.05<\phi<0.12$ and UCS>80	
(11)	$3.87\exp(1.14 \times 10^{-10} \rho V_p^2)$	Gulf of Mexico	–	
(12)	$46.2\exp(0.027E)$	–	–	
(13)	$2.28+4.1089E$	Worldwide	–	Bradford et al. (1998)
(14)	$254 (1-2.7\phi)^2$	Sedimentary basins worldwide	Very clean, well-consolidated sandstones with $\phi b0.3$	Vernik et al. (1993)
(15)	$277\exp(-10\phi)$	–	Sandstones with $2<UCS<360MPa$ and $0.002<\phi<0.33$	

2.5   Dynamic Properties

Dynamic elastic moduli of formation, Young's Modulus (E_{dyn}) and Poisson Ratio (ϑ_{dyn}), are independent, while shear and bulk moduli can be deduced from $Edyn$ and ϑdyn. The most important method for estimation of elastic parameters is acoustic logging and, in particular, acoustic wireline logs (Fjaer et. al., 2008). Given the compressional velocity (v_p), shear-wave velocity (v_s), and bulk density (ρ_b), E_{dyn} and ϑ_{dyn} can be calculated using the sonic based correlations (Fjaer et. al., 2008, Mavko et al., 2003, Lacy L. Lewis 1997).

The dynamic elastic properties are measured by sending an ultrasonic acoustic signal through a rock sample and measuring its velocity. The acoustic signal generates two types of waves, viz, compressional (longitudinal) and shear (transverse) waves. Therefore, the two velocities, vp and vs, are measured from a standard dynamic testing. These measurements are usually made simultaneously with the static measurements described above. E_{dyn} and ϑ_{dyn} are determined from rock physics relationship shown below, Hamid et al 2015:

$$E_{dyn} = \frac{\rho_b v_s^2 (3v_p^2 - 4v_s^2)}{(v_p^2 - v_s^2)} \qquad \textbf{Eq. 16}$$

$$\vartheta_{dyn} = \frac{(v_p^2 - 2v_s^2)}{(v_p^2 - v_s^2)} \qquad \textbf{Eq. 17}$$

Dynamic properties are correlated to the static properties, which are needed for most geomechanical model applications.

2.6   Static Properties

In triaxial tests, the static elastic properties measure the amount of strain by measuring deformation experienced by a rock sample when stress is applied. Before reaching peak stress level, the rock behavior is linearly elastic and is described by E and ϑ. Figure 4 shows axial and radial stress-stain responses measured on a core plug during a triaxial test. Permanent deformation occurs when the sample is subjected to axial stress beyond yield stress. Figure 5 defines static Poisson's ratio (ϑ_{sta}) as the ratio of radial and axial stains, εr and εa, and static Young's Modulus (E_{sta}), as the ratio of applied axial stress σa and resultant axial strain εa.
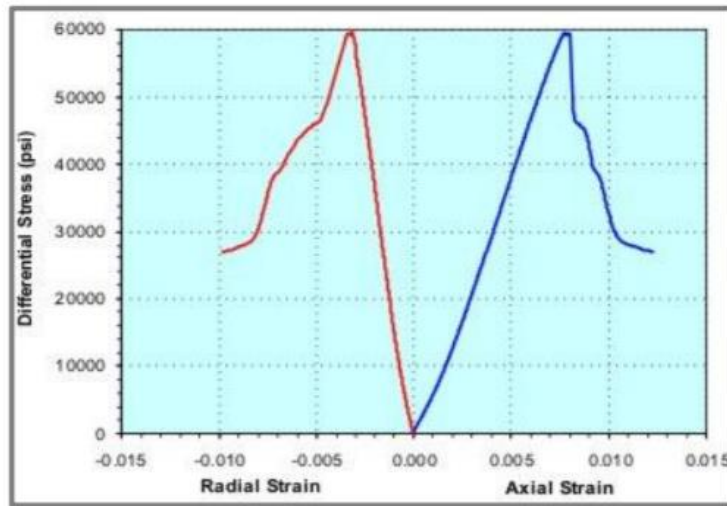

Figure 4 Radial and axial stress-strain response during a triaxial test (Hamid and Rahim 2015)
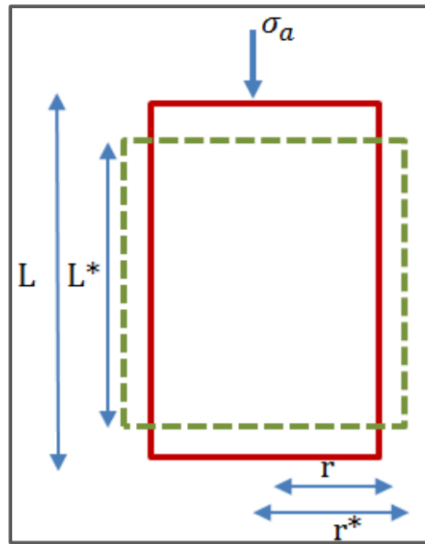
Axial Strain
$$\varepsilon_a = (L - L^*)/L$$
Positive

Radial Strain
$$\varepsilon_r = (r - r^*)/r$$
Negative

Poisson's Ratio
$$\vartheta = {-\varepsilon_r}/{\varepsilon_a}$$

Young's Modulus =
$$E = {\sigma_a}/{\varepsilon_a}$$

Figure 5 Elastic rock properties: Young's Modulus and Poisson's ratio during uniaxial test (Hamid and Rahim 2015)

Mohr-Coulomb failure criterion has been proposed to describe rock strength under different loading conditions. Figure 4 shows linear Mohr-Coulomb failure envelope in τ and σn space (a) and σ_1 ' & σ_2 ' space (b) These criteria can be expressed in two ways depending on the space, when plotting τ versus σn, yielding the following expression,
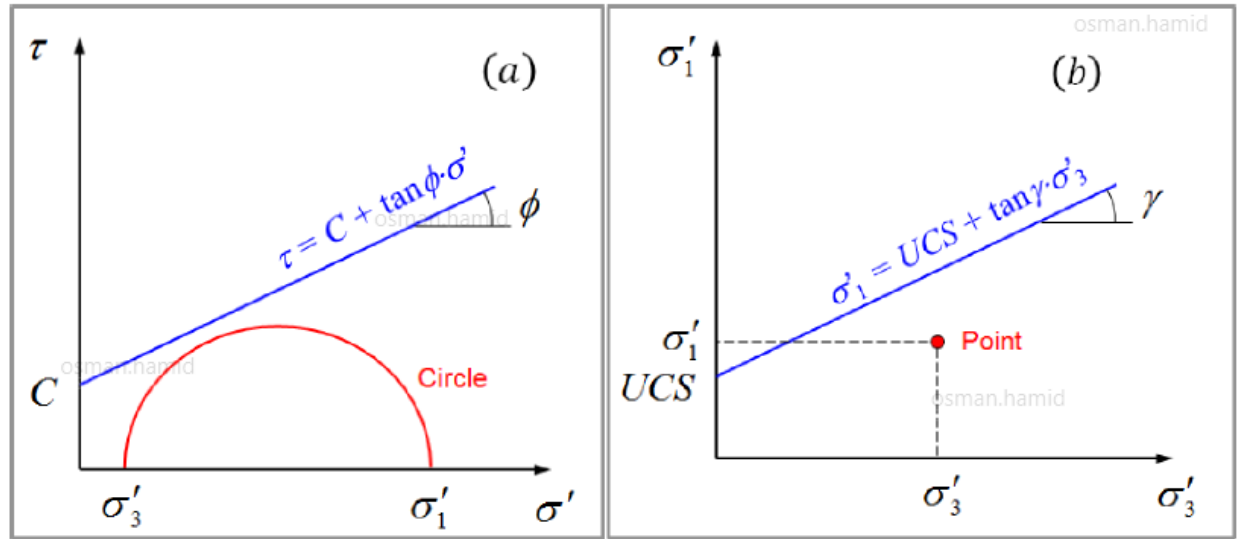
Figure 6 Linear Mohr-Coulomb failure envelope in shear stress (τ) and normal stress (σ_n) space (a) and effective stresses (b) (Hamid and Rahim 2015)

Fig. 6 shows linear Mohr-Coulomb failure envelope in τ and σn space (a) and σ_1' & σ_3' space (b) These criteria can be expressed in two ways depending on the space, when plotting τ versus σn, yielding the following expression,

$$\tau = C + Tan\emptyset.\,\sigma\,' \quad \textbf{Eq. 18}$$

and when plotting $\sigma 1\,'$ versus $\sigma 3\,'$, yielding the following expression.

$$\sigma_1' = UCS + Tan\gamma.\,\sigma_3' \quad \textbf{Eq. 19}$$

Where:

$\tau = shear\ stress\ at\ compressive\ yield$

$C = Cohesion$

$\sigma\,' = normal\ effective\ stress$

$\emptyset = Friction\ angle$

σ_1' & σ_3' = maximum and minimum effective principle stresses respectively

UCS = Unconfined Compressive Strength

$\gamma = (1 + \sin\emptyset)/(1 - \sin\emptyset)$

Mohr-Coulomb failure criterion has been proposed to describe rock strength under different loading conditions.

Domenico (1977) measured acoustic velocities under hydrostatic pressure in a sand and in glass beads of similar grain size and porosity. The velocity, pore volume, porosity, and pore compressibility as functions of pressure found for the dry and brine saturated sample are useful for a better understanding of unconsolidated formations. Wang (2002) measured velocity anisotropy under hydrostatic pressure in the lab on sands, shales, and rocks. A relation to estimate v_p anisotropy from v_s anisotropy and vice versa was found. However, as all these correlations have been measured under hydrostatic pressure, they have to be carefully extrapolated to in situ stress.

2.7 Finite Element

The finite element numerical method provides an analytical model which should be able to resolve many of the variables that related to rock mechanics. The model can be visualized as an array of finite parts (or blocks) in order to be represented as a rock mass. Equations predicting the behavior of each finite element are established, and then the equations for all elements are solved simultaneously. Thus, a digital computer is required because of the large number of elements that included in most of the outputs.

David (2010) showed how geomechanics can be modeled and mapped. Also, basic equation of iterative coupling between geomechanics where clearly identified.

2.7.1 Mapping Reservoir Grid to Finite Element

Information that originates with the reservoir grid (fluid pressure, temperature, initial porosity) needs to be transferred to the finite elements so that displacements can be computed. For a single-grid system, the mapping is one-to-one, so the pressure and temperature on a reservoir grid can be applied directly to a geomechanics grid. However, for a dual-grid system, the topology of the reservoir grid blocks must mapped correctly the topology of the finite elements, and vice versa. The following mapping shows how to transfer the values of variables of a reservoir grid block to a node of finite element.

2.7.2 Mapping Finite element to Reservoir Grid

Before performing the mapping, locations must be determined for the reservoir grid block center and corners with respect to the finite elements. This is done so the deformation and stress for reservoir grid blocks can be estimated from the geomechanics FE-based solution. When a reservoir grid block corner does not lie within any finite element, there is no deformation at the corner.

CHAPTER 3

METHODOLOGY

3.1   Proposed Work Plan

Field data will be used for 15 wells that already producing from the same sandstone reservoir. The data will be screened and filtered based on availability and quality to capture the needed data to build the 1D and then 3D model. After that, the data and the resulting model will be used to enhance future drilling operations and production forecasting prediction. At later stage, the answers of the below questions will be addressed:

1. How geomechanical changes in stress/strain impact wellbore stability related issues and drilling operations?

2. How much stress rotates around faulted zones?

3. How depletion effect hydraulic fracture growth?

3.1.1 Phase I: Data collection and Quality Check

The below reservoir and drilling data will be utilized:

- Reservoir pressure (From MDT and SBHP)

- Open hole Logs

- Deviation surveys

- Seismic data

- Mud reports

- Core data

- Mini-frac results

3.1.2 Phase II: Building 1D and 3D Geomechanical Models

• Building a calibrated 1D geomechanical model, including mechanical properties-using rock physics, pore pressure, using velocity to pore pressure transform and principal in-situ stresses-using poroelastic models for minimum horizontal stress, depending on stress regime of the area, overburden stress from bulk density measurements, maximum horizontal stress need special data and methodology.

• Grid construction

• Constructing a 3D geomechanical model by populating properties using appropriate geostatistical methods, such as kriging interpolation or Gaussian function.

• Computing anisotropic properties if data available (fault included).

• Conduct pre-depletion modeling using finite element method and calibrate the resultant stresses against calibrated 1D model to validate the boundary conditions.

• Conduct depletion runs (isotropic/anisotropic) using different scenarios of injection pressure-couple reservoir and geomechanical modeling.

Interpretation of Finite Element modeling results:

Determination of minimum and maximum injection pressure to ensure integrity of reservoir and surrounding formation.

• Stress path analysis.

• Changes in magnitude and orientation of stress.

• Displacement orientation.

• Plastic volumetric strain.

3.1.3 Phase III: Effect of Depletion on Wellbore Stability and Hydraulic Fracturing

After identifying the effect of pressure depletion on both wellbore stability and hydraulic fracturing, will have better understanding of the cap rock which will lead to have enhancement in future drilling operations and production forecasting prediction.

CHAPTER 4

ROCK PHYSICS

4.1 Introduction

Understanding elastic rock mechanics behaviors and rock strength are required for various oilfield operations, such as drilling, stimulation and production operations. Building a perfect geomechanical model mainly depends on rock mechanical parameters including elastic modulus and rock strength. Wellbore stability modeling is essential for drilling a save wellbore to TD without experiencing any stability related issues; this modeling depends on understanding stresses, pore pressure and mechanical properties of investigated section. Hydraulic fracture modeling on the other hand depends on the mechanical behavior of the rocks, such as Young's modulus and Poisson's ratio, solid production strategies based on the magnitude of the unconfined compressive strength beside other geomechanical factors.

Elastic properties such as Young's modulus (E), Poisson's ratio (ϑ), rock strength, and the variation of in-situ stresses are required to provide quantitative analyses for geomechanical modeling. Rock mechanics data can be estimated from wireline logs such as sonic and density logs; these log measurements are, to some extent, related to the mechanical properties of formations or can be measured in the laboratory using uniaxial, triaxial, or ultrasonic tests.

The variability in the mechanical behavior measured in the core plugs in the study area makes such operations extremely challenging. Using available triaxial testing results including static and dynamic properties E and ϑ, rock strength such as unconfined compressive strength (UCS) and friction angle (FANG) together with petrophysical properties, such compressional and shear velocities, density and porosity to derive related rock physics correlations.

4.2 Rock Physics

Qui et al., 2013 indicated that sonic data and petrophysical properties correlations usually derived from specific rock type, age, depth range, and field, and their applications to other rocks may not be reliable unless calibrated with specific field's conditions. **Fig.7** shows a plot of density (ρ_b) versus p-wave velocity (V_p) for Reservoir A sandstone where the core data plotted along with Mavko et al., 2003 correlation and is showing good fit.
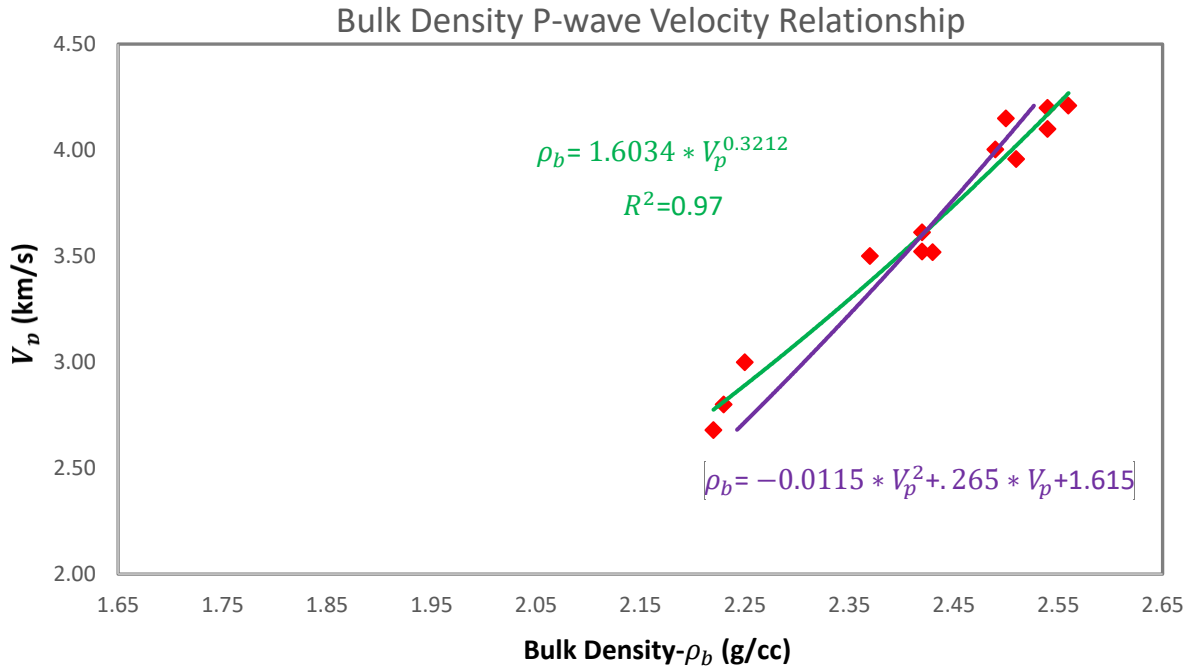
Mavko et al., 2003

$\rho = -A * V_p^2 + B * V_p + C$ **Eq. 20**

$\rho_b = -0.0115 * V_p^2 + .265 * V_p + 1.615$ **Eq. 21**
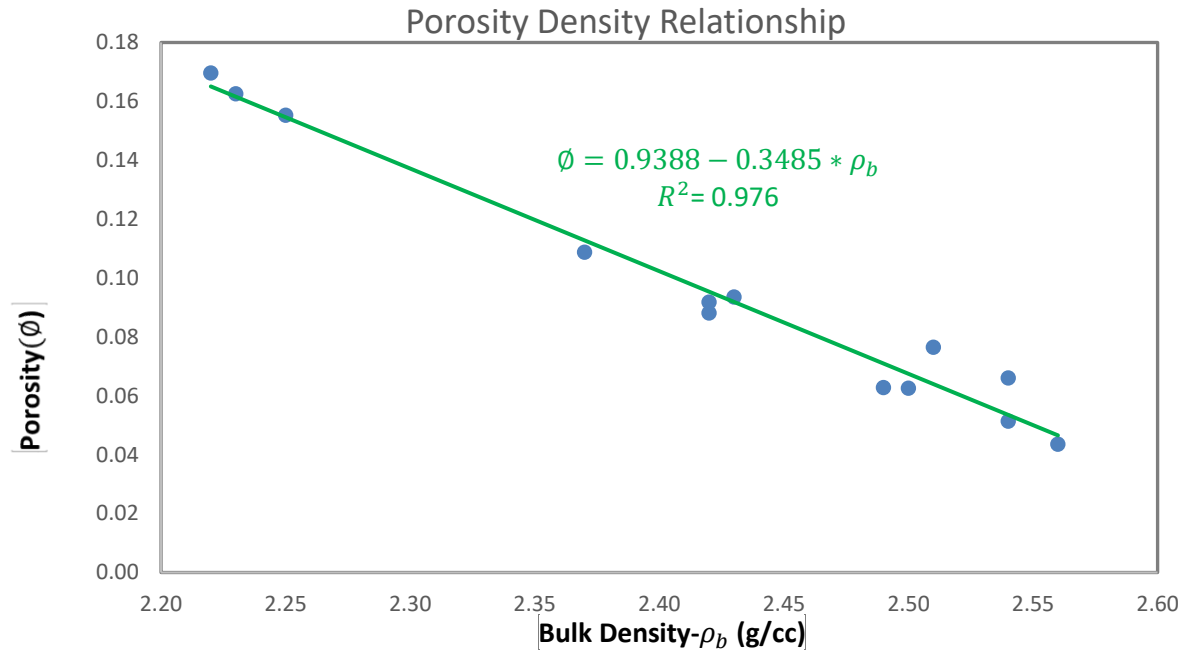
$\rho_b = 1.6034 * V_p^{0.3212}$ **Eq. 22**

Density velocity correlation, Density in g/cc and velocity in km/s:

Figure 7 Density (ρb) versus p-wave velocity (vp)

Fig.8 shows a plot of density (ρb) versus porosity (ϑ) for Reservoir A Sandstone which indicates that there is a good correlation.

$$\emptyset = 0.9388 - 0.3485 * \rho_b \quad \textbf{Eq. 23}$$

Porosity Density Relationship

$$\emptyset = 0.9388 - 0.3485 * \rho_b$$
$$R^2 = 0.976$$

Figure 8 Density (ρb) versus Porosity ($\emptyset$)

The Relationship between V_p and V_s is illustrated in **Fig.9** using Castagna et al., 1993 & Mavko et al., 2003 equations.

Mavko et al., 2003 $\qquad\qquad\qquad\qquad V_s = 0.754 * V_p - 0.657$ **Eq. 24**

Castagna et al., 1993 $\qquad\qquad\qquad\qquad V_s = 0.8042 * V_p - 0.8559$ **Eq. 25**

Best Fit $\qquad\qquad\qquad\qquad\qquad\qquad V_s = 0.87765 * V_p - 0.809$ **Eq. 26**
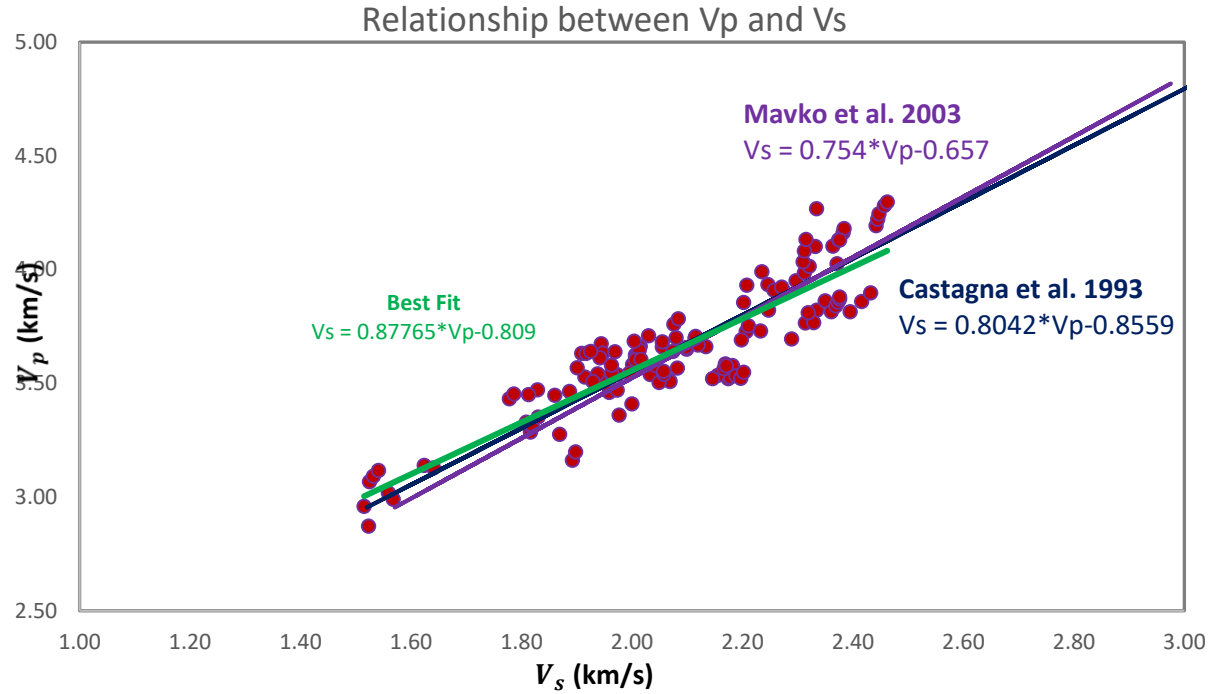
32

Figure 9 Vp versus Vs Relationship

4.3 Dynamic to Static Young's Modulus Transform

The majority of laboratory-measured data collected were static measurements while a limited number of dynamic measurement data such as velocity measurements were available in some source. The static mechanical properties are usually estimated from calibrated correlations functions using dynamic elastic parameters, which are mainly calculated from sonic and density logs. In this study, static and dynamic properties were determined from triaxial core test for Reservoir A. Typical correlations between $\vartheta dyn\ and\ \vartheta sta$ is shown in **Fig.10.** This figure depicts cross plot of measured $\vartheta dyn\ and\ \vartheta sta$ and different ratios of static to dynamic Poisson's ratio for Reservoir A.

Fig.11 shows the relationship between $Edyn\ and\ Esta$. **Fig.11** demonstrates that the static values of Young's modulus are related to dynamic values by the following equation:

$Esta = 0.8029* Edyn - 0.1666$ **Eq. 27**
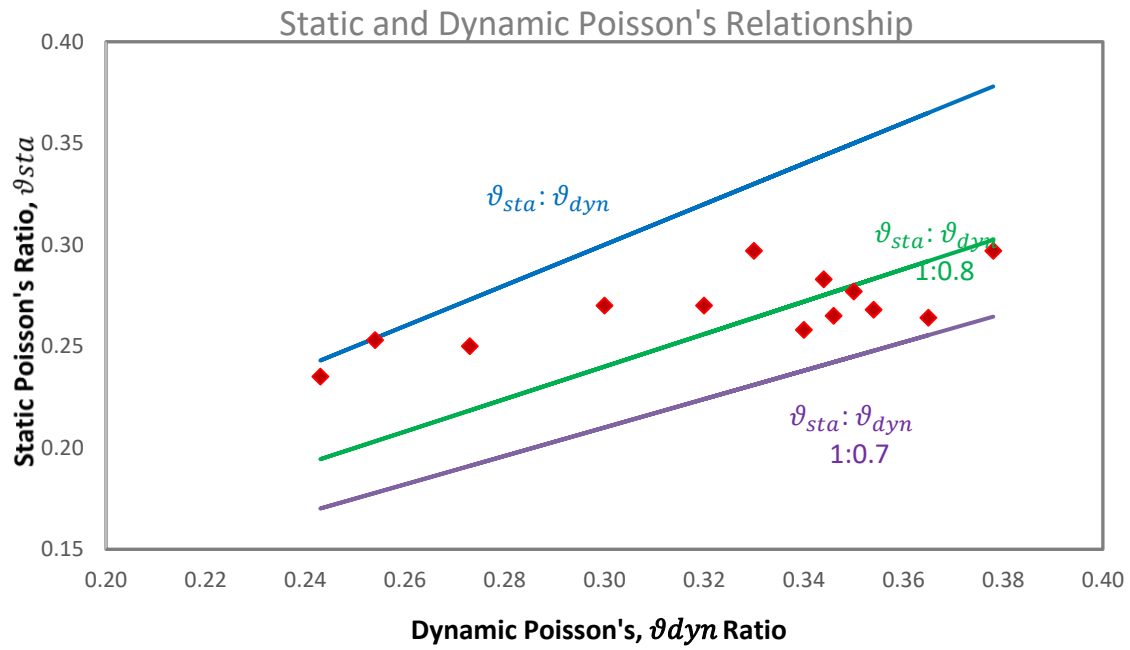

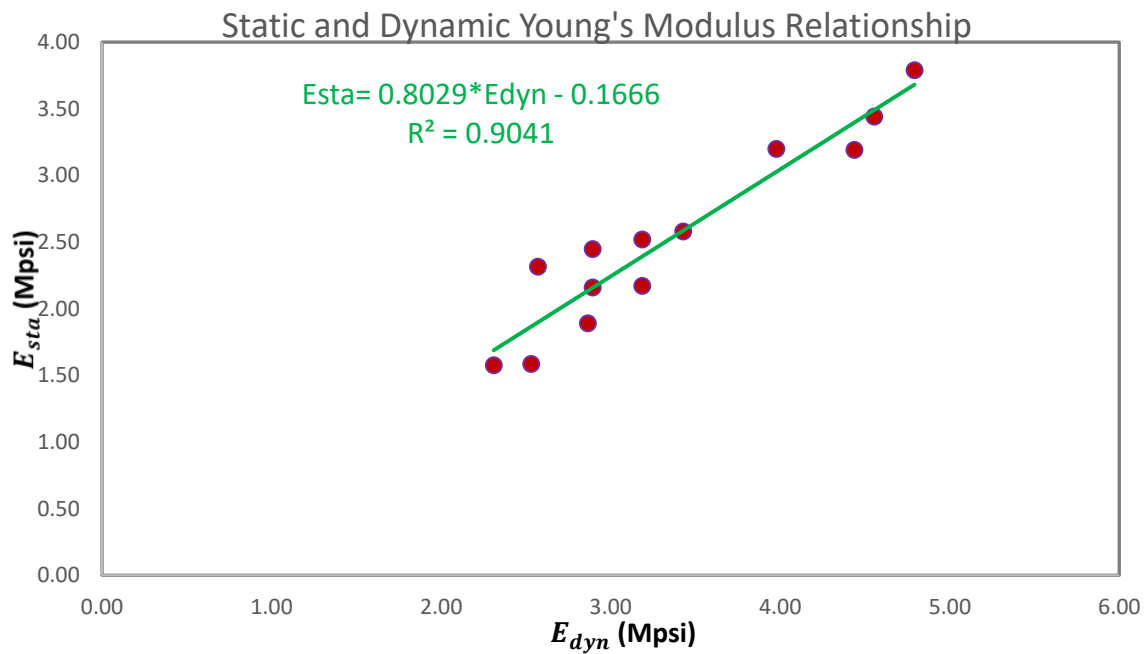**Figure 10**   **Static and Dynamic Poisson's Relationship**

Figure 11   **Static and Dynamic Young's Modulus Relationship**

4.4 Empirical Rock Strength Relationship

In **1987, McNally** obtained the relationship between UCS and the compressional slowness DTCO for sandstone reservoir rocks. **Fig.12** represents Reservoir data plotted from McNally eqn. and the correlation from the data itself.

McNally 1987
$$UCS = (1200\exp(-0.036\Delta t_c))*145.037738 \quad \textbf{Eq. 28}$$

$$UCS = 5E + 08 * \Delta t_c^{-2.467} \quad \textbf{Eq. 29}$$

The relationships between UCS and static Young's modulus *Esta* plotted along with **Bradford et al. 1998** correlation, for rocks typically encountered in sandstone reservoirs is illustrated in **Fig.13** for Reservoir A.

Bradford et al. 1998
$$UCS = 2.28 + 4.1089 * E_{sta} \quad \textbf{Eq. 30}$$

$$UCS = 3386.9 * E_{sta}\text{-}450.3 \quad \textbf{Eq. 31}$$

Fig.14 illustrates relationship between UCS and Porosity for Reservoir A. Where UCS is in psi, and DTCO in μs/ft.
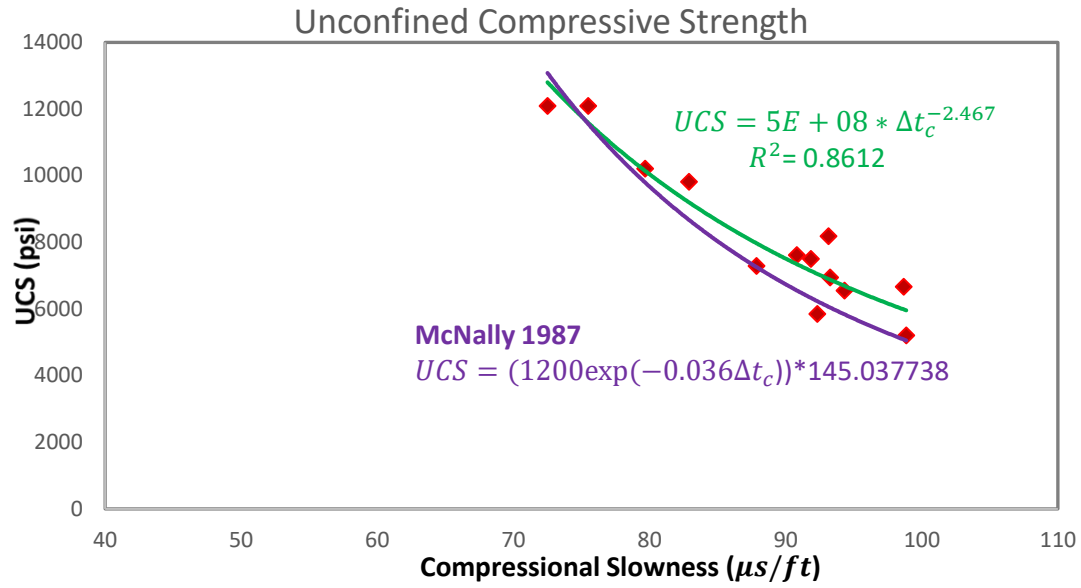
Figure 12   **UCS versus Compressional Slowness**
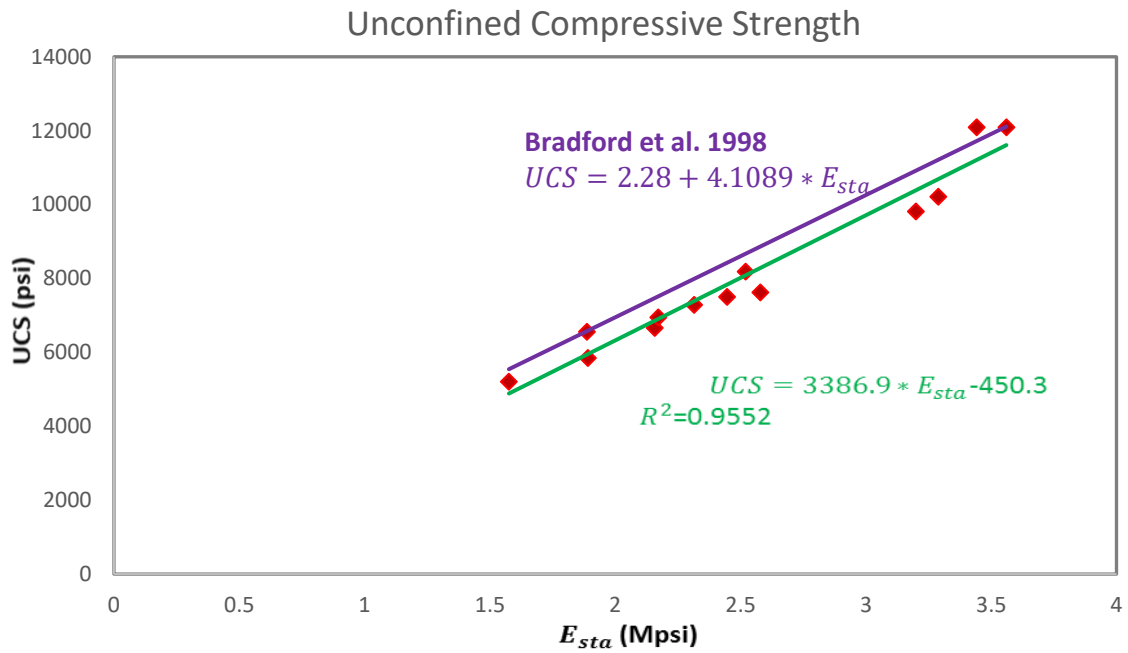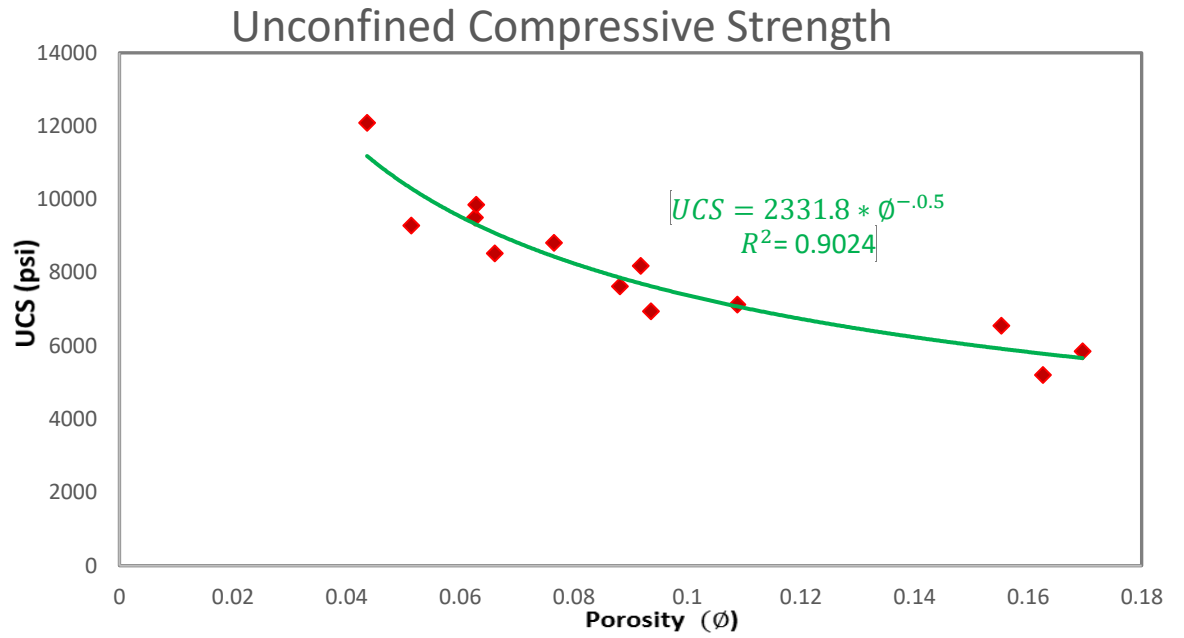

Figure 13   **UCS versus Static Young's modulus, Esta**

Figure 14   UCS versus Porosity Relationship

The rock friction angles (FANG) are obtained from slopes of Mohr envelopes drawn as a tangent to the Mohr circles (Turk and Dearman, 1986).

Fig.15 show the relationships between FANG and V_p plotted along with Lal (1999) correlation. The best fit line for Reservoir is given by the following equation.

Lal 1999

$$FANG = sin^{-1}\{(V_p - 1)/(V_p + 1)\} \textbf{ Eq. 32}$$

$$FANG = 18.597 * V_p - 1.4054 * V_p^2 - 10.997 \textbf{ Eq. 33}$$

Where FANG is in degrees, and V_p in km/s.
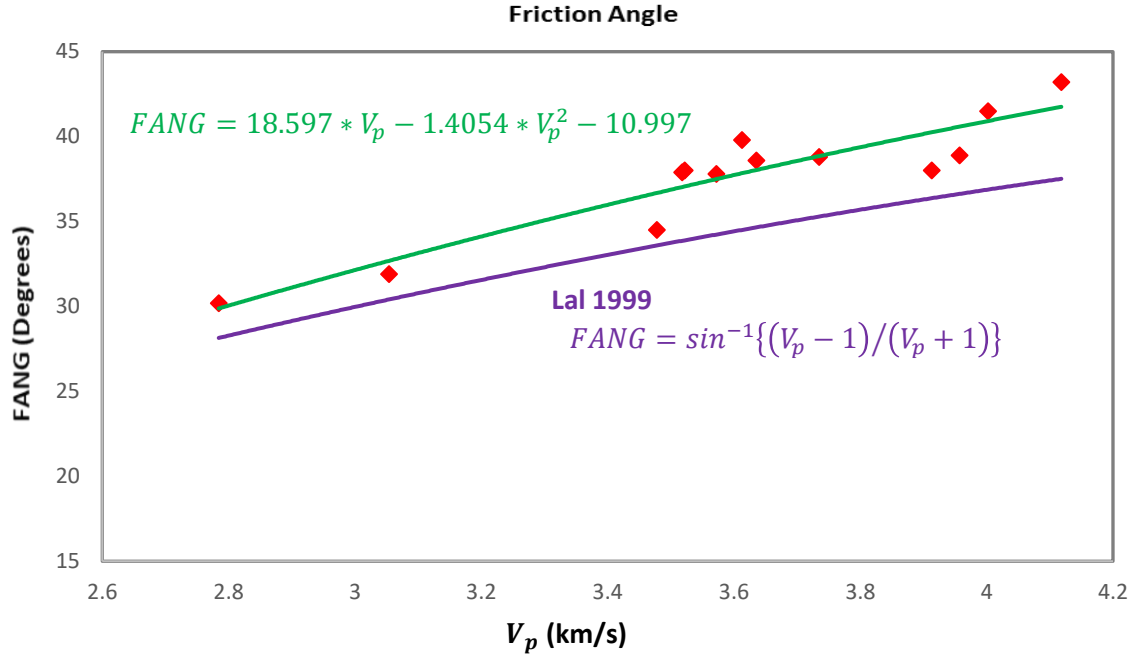
Figure 15　　　　**Friction Angle, FANG versus Vp Relationship**

The relationship between UCS and cohesion is calculated from the below equations and illustrated in **Fig.16.** (D. Moos et al 2007)

$$\beta = 45 + \frac{\emptyset}{2} \qquad \textbf{Eq. 34} \qquad\qquad \tan\gamma = \tan^2\beta \qquad \textbf{Eq. 35}$$

$$\sin\emptyset = \frac{\tan\gamma - 1}{\tan\gamma + 1} \qquad \textbf{Eq. 36} \qquad\qquad \tan\gamma = \frac{1 - \sin\emptyset}{1 + \sin\emptyset} \qquad \textbf{Eq. 37}$$

$$\text{UCS} = 2C\tan\beta \qquad \textbf{Eq. 38} \qquad\qquad C = \frac{\text{UCS}}{2.\tan\beta} \qquad \textbf{Eq. 39}$$
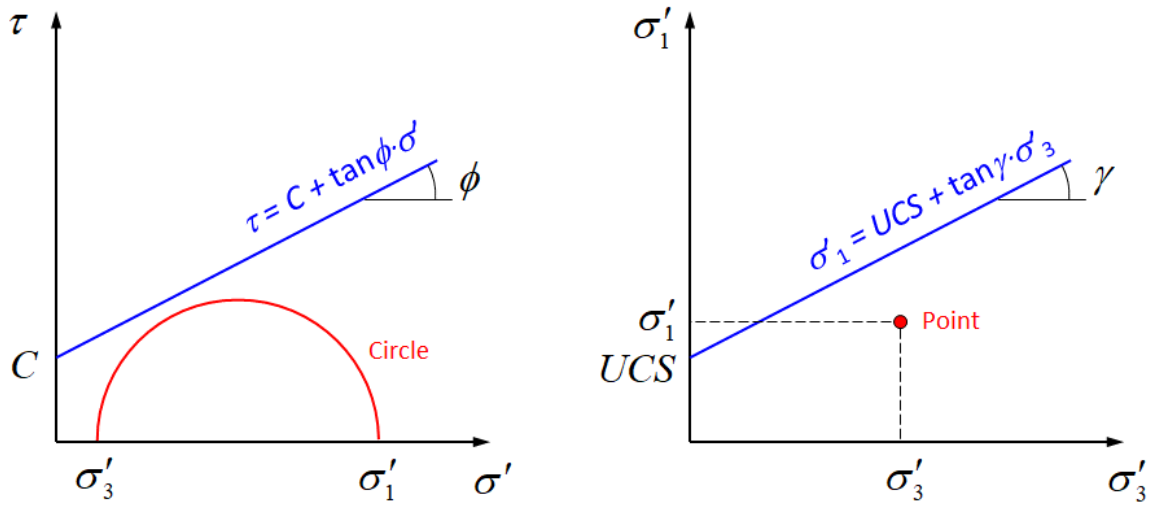
Figure 16   **UCS and Cohesion relationship**

CHAPTER 5

MODEL & RESULTS

5.1 Building 3D Geomechanical Model

The formation of interest in the study area are Sandstone. These surfaces along with several intermediate surfaces are included to increase the vertical resolution of the 3D static model. The following section discusses the static model building using the seismic horizons and other relevant data.

Data available for static model building are as follows.

- Results from 1D geomechanical models and wellbore stress analysis from offset wells (15 Wells)
- Interpreted surfaces of Sandstone and Base of the formation.

**Fig.17** shows a map view of the main horizons and three offset wells. The interval of interest for the analysis covers multiple sandstone formations. To capture more details of the rock properties, this interval was further divided into sub zones. The grid was coarsened by extending to ground level and sideburden and underburden was also added. The total number of grid cells in the final 3D geomechanics model is 7.6 million.
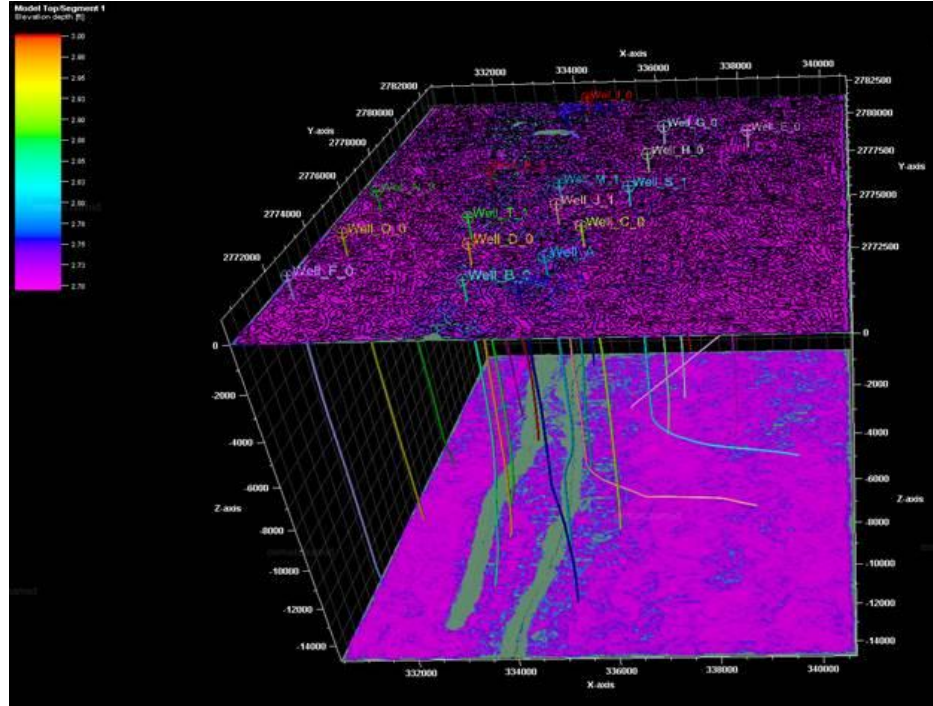
Figure 17   **Position of offset wells along with overburden and reservoir horizons**

Continuous properties curves at log resolution were available for the offset wells that included critical data such as static Young's modulus and Poisson's ratio, bulk density, unconfined compressive strength, and friction angle.

Using different functionalities in the software, the logs were upscaled to the 3D model. The upscaled logs for all the offset wells were interpolated throughout the 3D model. This interpolation was performed using Sequential Gaussian Simulation. The entire 3D model that included the reservoir, underburden, and overburden in intervals was then populated with the mechanical properties from the calibrated 1D geomechanical models. **Fig.18** shows a 3D and spatial distribution of Young's modulus at Sandstone formation levels. Similarly, Poisson's ratio in **Fig.19**, density in **Fig.20,** compressional velocity in **Fig.21** and shear velocity in **Fig.22** were distributed in the 3D space.

41
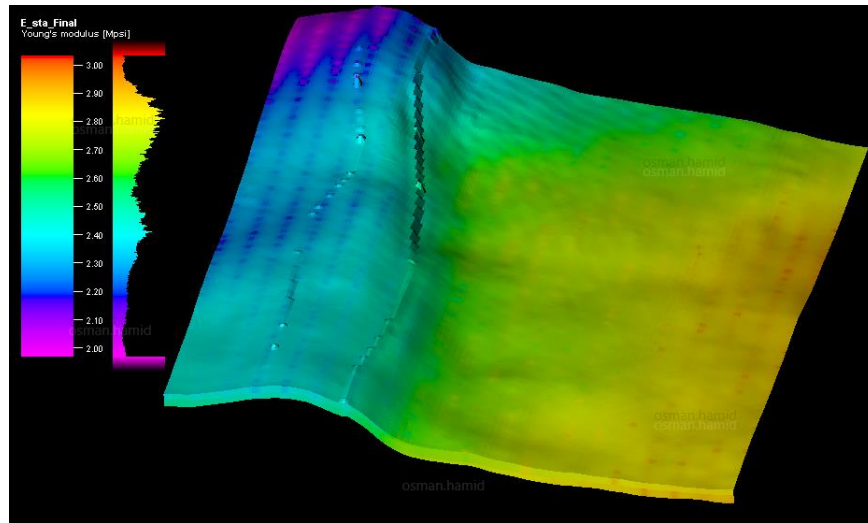
Figure 18   **3D distribution of Young's modulus**
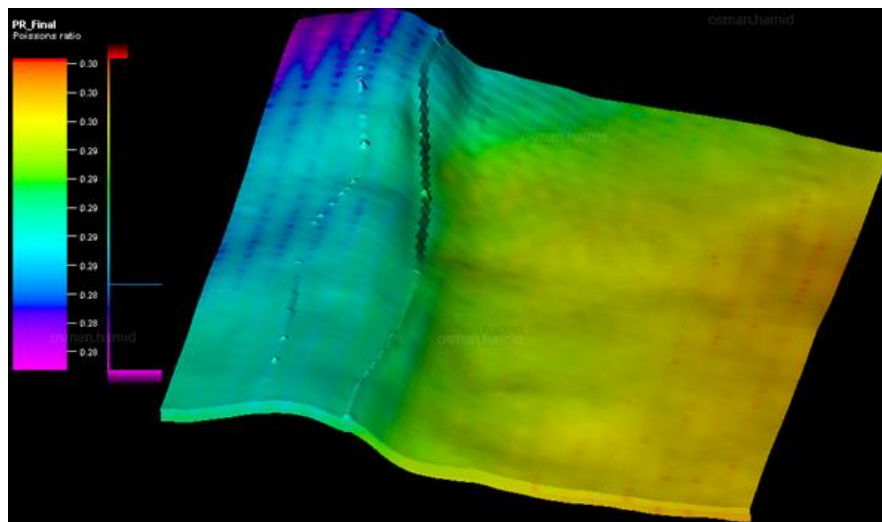
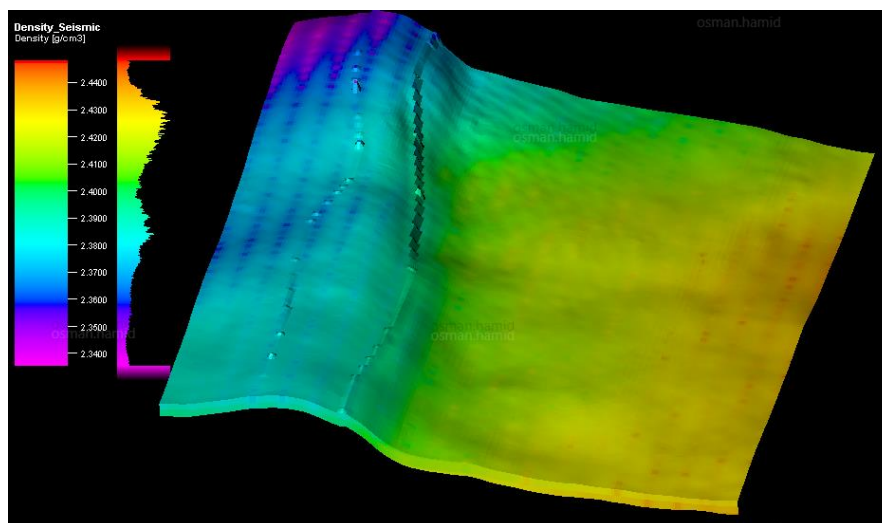**Figure 19**   **3D distribution of Poisson's ratio**

Figure 20   3D distribution of Density Seismic
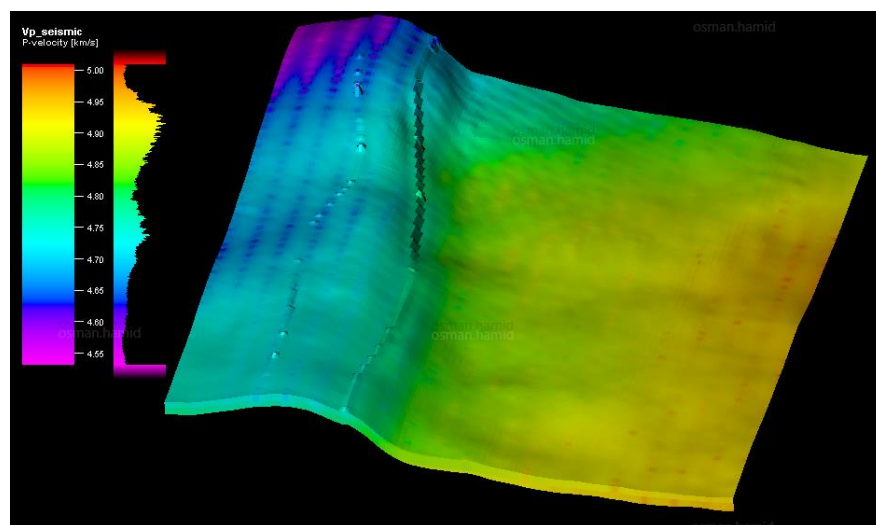
Figure 21   3D distribution of Compressional Velocity
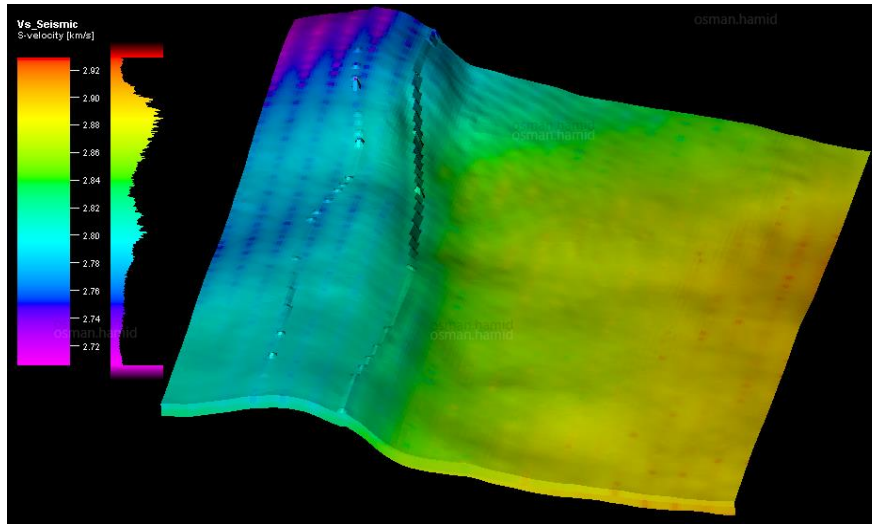
Figure 22　　　　**3D distribution of Shear Velocity**

5.2 Embedding

The process of embedding the reservoir with underburden and sideburden was commenced

after obtaining a reasonable finite element mesh for the reservoir. Embedding is an

essential method to ensure that boundary effects do not affect the stress state in the area of

interest, **Fig. 23**. The side-burden was created such that the edge of the model is at least

three times the reservoir width away from the reservoir itself and orthogonally aligned with

the global coordinate system. The underburden thickness was chosen such that the resulting

model is roughly cubical in shape. A single-material simulation was performed prior

commencing the 3D geomechanics modeling process, where default properties are

assigned to all cells in the complete model, to check grid functionality and that the linear

stress gradients are calculated when properties do not vary (Hamid., 2015).
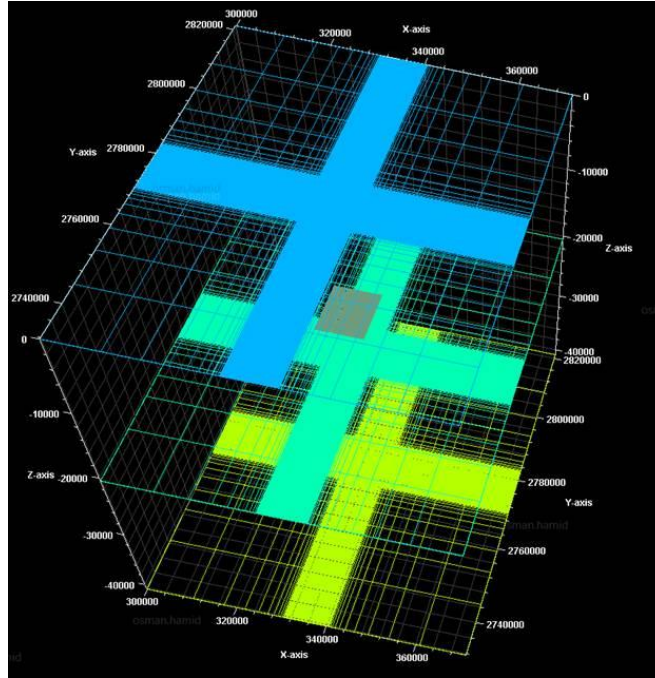
Figure 23   Final embedded model grid

5.3 Stress Calculation

The stress initialization considers gravity and pore pressure forces acting internally on the model and an external horizontal loading acting on the model boundaries to represent σ_{min} and σ_{max}. The advantage of such a scheme to assign boundary conditions is that a complex stress state can be calculated within the model to represent the model's in-situ effective stress state in a realistic manner, as it accounts for the geomechanical property distributions and the shape of the model layers. The pore pressure in all Sandstone layers was estimated using the pore pressure profiles from 1D geomechanical models of fifteen offset wells.

The first step of the stress modeling is the calculation of stresses due to gravity. Gravitational forces act on each cell according to its assigned density, with sliding boundary conditions at the sides of the model. The assigned pore pressure gradient helps to support the weight of the overburden as depth increases. The result of this first model

run is a stress state for the whole grid that reflects density and topography variations (Hamid, 2015).

The pore pressure and gravity step is followed by another simulation where far-field horizontal stresses are applied to the model boundaries. On each side boundary, vertical gradients of σ_{min} and σ_{max} are assigned with an orientation for the maximum that reflects what is known of the regional tectonic conditions.

The stress simulation uses the internal density, pore pressure properties, and the external horizontal stress conditions to calculate the local stress field in each grid cell as previously
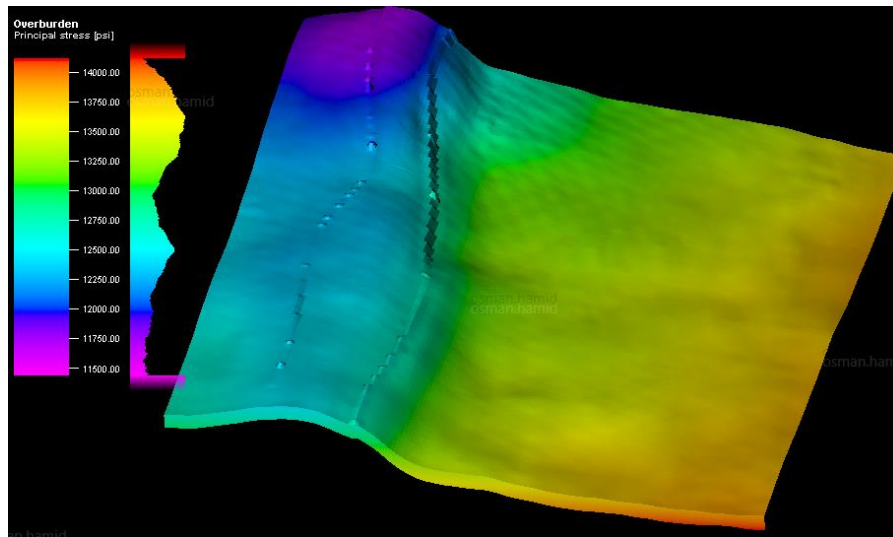
Figure 24   3D distribution of Overburden Stress

shown. The elastic properties, as well as the Mohr-Coulomb properties, influence the final distribution of the in-situ stresses. The local stress concentrations and stress rotations can result from abrupt changes of elastic properties at stratigraphic boundaries. Details about the 3D geomechanics algorithm can be found in Koutsabeloulis & Hope (1998).

Fig. 24 shows the 3D distribution of Overburden Stress which range from 11,500- 14,000 psi.

However, **Fig. 25 & 26** indicate the scenario pore pressure prediction from 2017 to 2038.

In 2017, the pore pressure is ranging from 6,600 to 7,800 psi while in 2038 it depleted to

the range of 3,300 to 3,900 psi across the field.
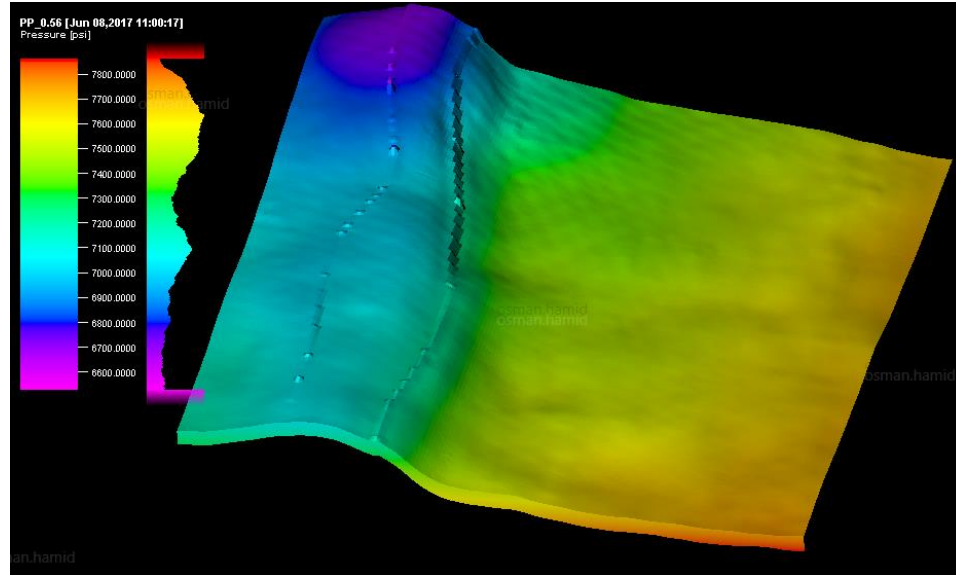
Figure 25   **3D distribution of Pore Pressure in 2017**
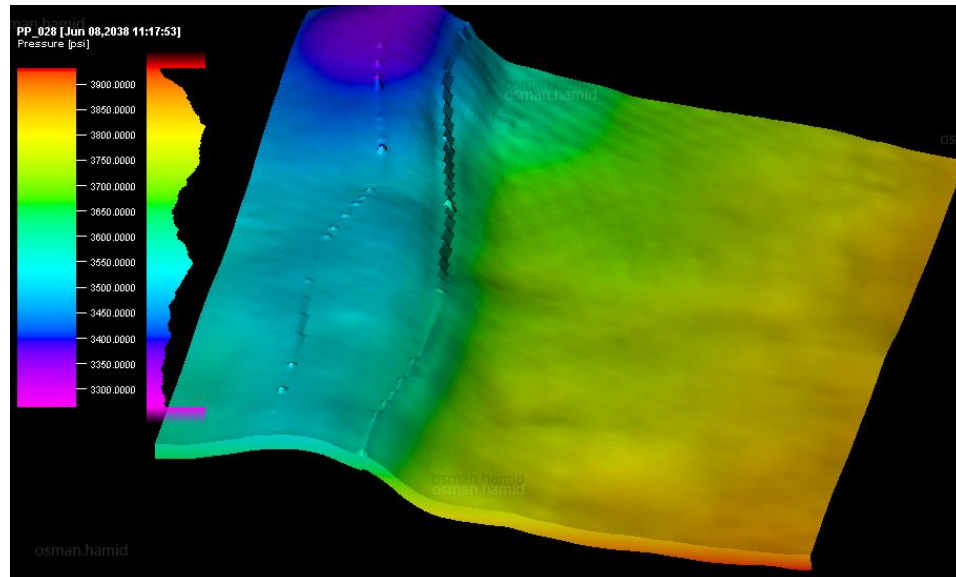
Figure 26   **3D distribution of Pore Pressure in 2038**

5.4 3D MEM Results

The rock properties contained in the 1D geomechanical models constructed will be used to populate the 3D geomechanical models using geostatistic approaches. The results of the modeling create a 3D Geomechanical model representing the in-situ stress state, as it is present in the undisturbed underground, prior to drilling a well. This model provides stress magnitudes and stress directions for each grid cell. This section provides an overview of the main results of the full 3D geomechanical model.

In a 3D model, principal stresses are not identical to overburden and horizontal stresses, σ_v, σ_{Hmax} and σ_{min}, as the principal stresses do not need to be vertically or horizontally aligned, hence the definition of the two stress systems differs in a 3D model. However, for the ease of understanding of the 3D model results, the following can be assumed.

- Maximum principal stress ~ σ_{Hmax}
- Intermediate principal stress ~ σ_v
- Minimum principal stress ~ σ_{min}

5.5 Change in Stresses due to Depletion

It is known that stress magnitude in the reservoir decreases due to depletion. This decrease of stress in the reservoir causes increase of σ_H above and below the reservoir. The 3D geomechanics model is then used to simulate with this pressure profile. The change in horizontal stress at Sandstone layers showed that the σ_H decreased in the depleted zone but increased considerably around the depleted zone compared to far field stresses.

Another way to visualize the 3D stress field is to plot the stress tensors in one layer of the model. The magnitude and direction of the three principal stresses (maximum, minimum

and intermediate stress) are shown as small, colored arrows for each cell. The stress magnitude is encoded by the color and length of each arrow, and the direction by the angle of the arrow in space as **Fig.27** shows. In many locations, the three principal stresses can be considered equivalent to σ_{min}, σ_{max}, and σ_V, but in some locations they become inclined, and the stress orientation can be regarded as rotating between adjoining cells.
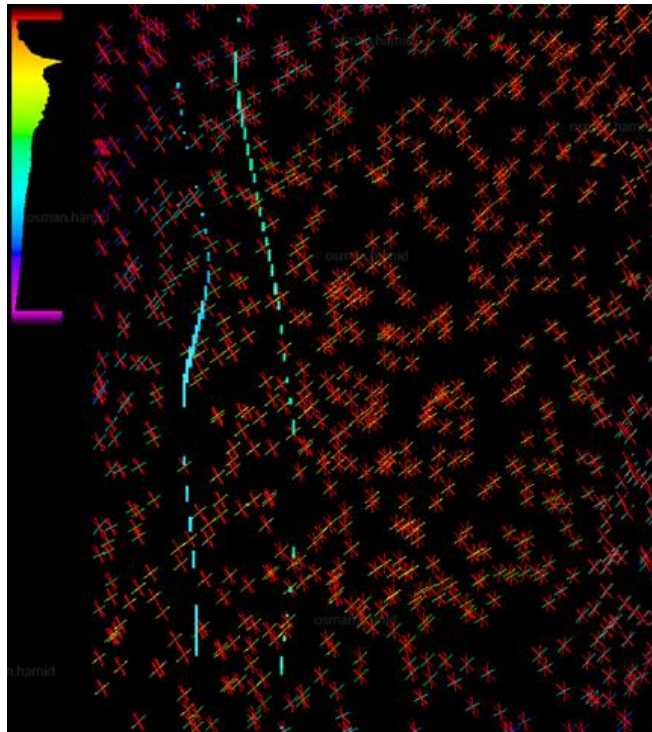
Figure 27   Stress orientation map

Fig.28 & Fig.29 & Fig.30 show the 3D distribution of Effective Stress from 2014 to 2038.

Based on the prediction runs from 2014 to 2038, The Effective Stress range changes from low to high stress due to depletion.
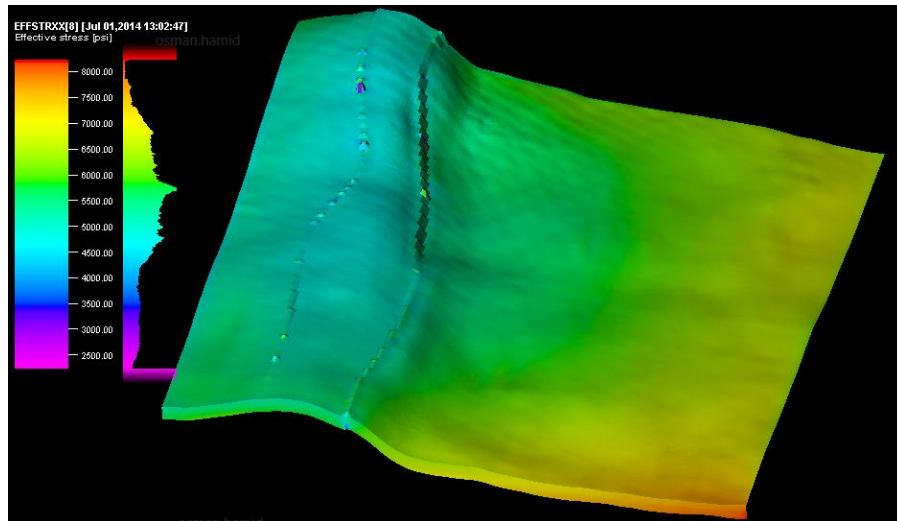
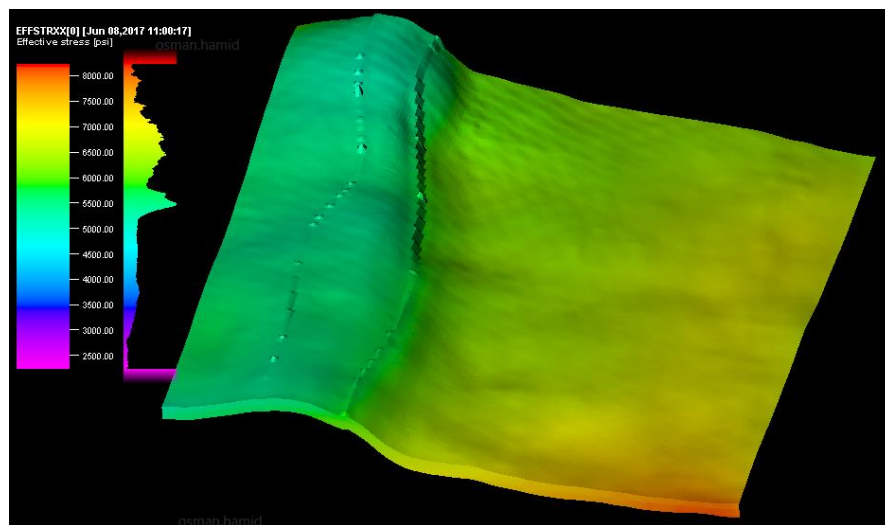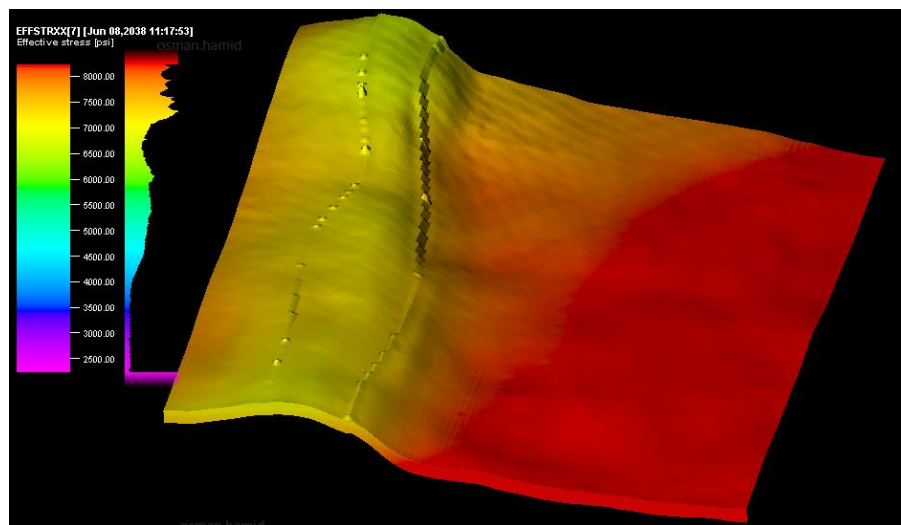**Figure 28**   **3D distribution of Effective Stress in 2014**

Figure 29   **3D distribution of Effective Stress in 2017**

Figure 30   **3D distribution of Effective Stress in 2038**

5.6 Hydraulic Fracture Model

In-situ stresses are the main influence on how hydraulic fractures propagate and take shape. In fact, in-situ stress differences that exist between layers governs the degree in which fractures are contained. Since stress contrast has the most significant control, an absence of it would lead other mechanism to contribute, such as slip on bedding planes and fracture toughness contrast. Furthermore, in order to predict the direction in which hydraulic fractures propagate, understanding the σ_{min} direction is necessary; since most of the time the propagation is in the σ_{min} direction away from the wellbore.

Stresses are functions of depth, lithology, pore pressure, structure, and tectonic setting. The stress regime in a given environment depends, therefore, on regional considerations (tectonics) and local considerations (lithology). Understanding the interaction between regional and local considerations is important as it controls the stress variations between layers. In some stress regimes the adjacent layers are under higher stress than the pay zone, enhancing fracture height containment; in others, the adjacent layers are under lower stress than the pay zone, and fracture propagation out of the zone is likely, limiting lateral fracture penetration.

It is proven that hydraulic fracturing is optimized in wells drilled in σ_{min} direction. In fact, it creates transverse hydraulic fractures that increase reservoir contact area, which in return improves gas production. In addition, it allows hydraulically induced fractures to connect with more natural fracture networks, if they exist. Even though transverse fractures help to increase production rates, it is more challenging to drill horizontally in the σ_{min} direction. This is due to the predominant stress magnitudes of σ_{max} and overburden σ_{ob} encountered

by the wellbore; with σ_{min} being the least in magnitude in a field that features a strike-slip stress regime.

The main inputs for planning a hydraulic fracture treatment are the proper evaluation of in-situ stresses, rock properties, and reservoir pressure. The stress, especially σ_{min} in the pay zone and upper and lower layers is the single most important fractor controlling hydracture fracture. It affects fracture orientation, fracture height, fracture width, treating pressure and proppant crushing and embedment. If the stress changes considerably in the pay zone and/or in the layers above and below due to depletion, then this change needs to be incorporated in the hydraulic fracture model. Hence, a proper stress estimation using 3D geomechanics could enhance the effectiveness of a hydraulic fracturing model.

5.7 Effects of Depletion on Hydraulic Fracture Geometry

Depletion could change the stress contrast between payzone and layers above and below, hence depletion could play a role similar to stress contrast. As the stress contrast increases due to depletion, the hydraulic fractures could be confined to the pay zone, become thinner, and longer. If the stress contrast is not very high, the hydraulic fractures could propagate across the adjoining layers resulting in pinchouts.

5.8 Hydraulic Fracturing Conceptual Case Studies

5.8.1 1st Case Studies

A conceptual case study was conducted to understand the effect of depletion and subsequent stress changes. One of the vertical wells was assumed, two depletion cases with different stress behavior. The required information for hydraulic fracture simulation was sampled across the vertical well trajectories from the 3D mechanical earth model.

Fig.31 displays the base case before depletion which show that the frac is tending to grow up. Moreover, **Fig.32 & 33** show the comparison of fracture width, proppant coverage and conductivity in both depletion cases using simulation.

Some of the output from both Scenarios are as follow:

- Scenario-A Pclosure = 8,969 psi gives gradient of 0.63 psi/ft.

- Scenario-B Pclosure = 8,304 psi gives gradient of 0.58 psi/ft.
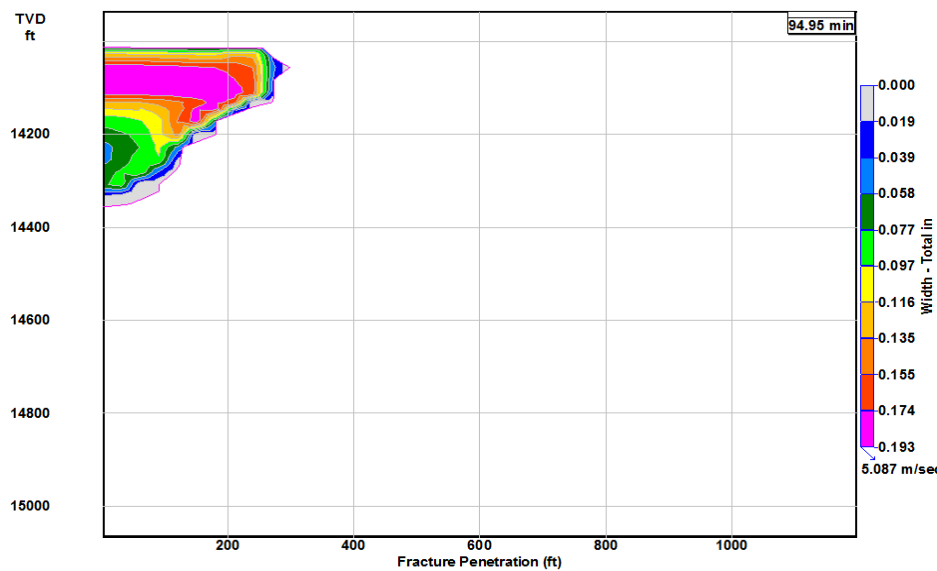
Figure 31   Hydraulic Fracturing 1st Base Case (No Depletion)

Table-2 shows the calculated results of the simulator which indicates the differences between the two cases such as the fracture length, conductivity which can visualized in the figures.

Using different stresses to show the effect of stress changes effect in Hydraulic Fracturing in the same well. In scenario A, the stress ranges from 8,000- 15,800 psi in the well and 8,000-10,000 psi in the studied formation. Furthermore, scenario -B stress ranges from 7,800- 14,000 psi in the well and 7,800-8,800 psi in the studied formation. Both case scenarios show that higher stress anisotropy can act as stress barrier. Also, the change in

stress due to depletion would stop the propagation of hydraulic fractures as both scenarios indicated comparing with the base case. As a result, in Scenario-A hydraulic fracturing half length is 401 ft while it is 366 ft in Scenario-B. Moreover, the propped length in Scenario-A is also greater by 35' than Scenario-B.

Table 2 Hydraulic Fracturing 1ˢᵗ Case Scenarios Results

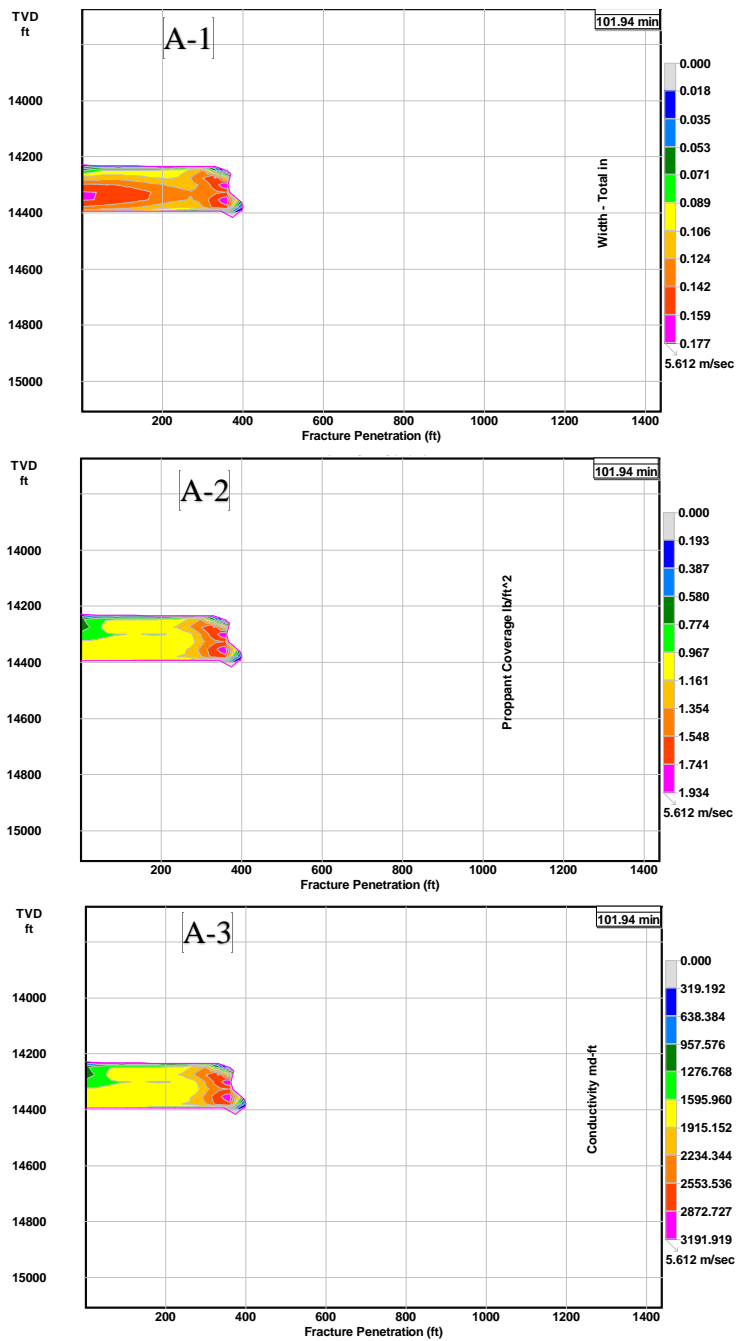| Hydraulic Fracturing Scenarios		Scenario-A Calculated Results	Scenario-B Calculated Results
Half Length	**'Hydraulic' Length (ft)**	401	366
	Propped length (ft)	397	362
PRESSURE:	**Max Net Pressure (psi)**	470	496
PROPPANT:	**Average In Situ Conc.(lb/ft^2)**	1	1
	Average Conductivity (md-ft)	1850	1925
	Fcd (KfW/k/Xf)	3	4
HEIGHT:	**Max Fracture Height (ft)**	164	166

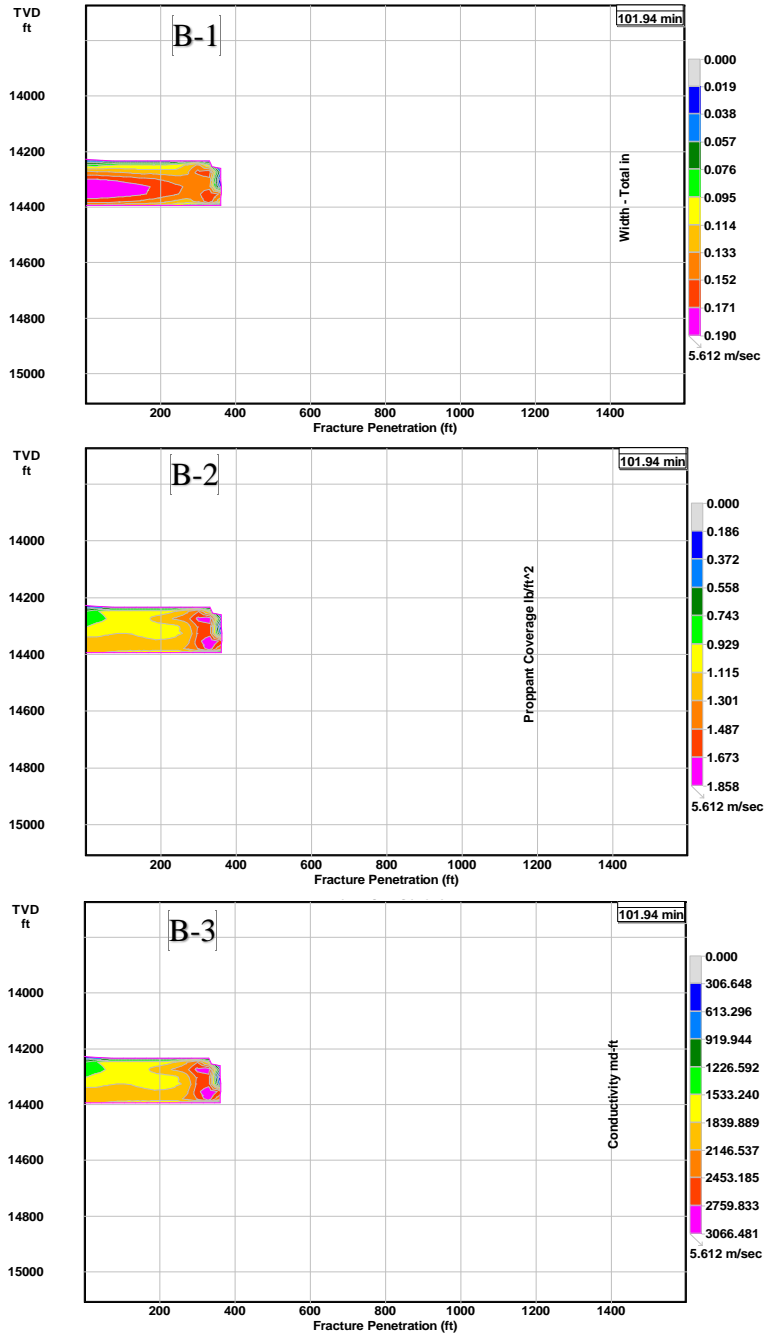**Figure 33**   **Hydraulic Fracturing 1st Case Scenario-A**   **Figure 32**   **Hydraulic Fracturing 1st Case Scenario-B.**

5.8.2 2nd Case Study

Another case study was conducted to validate the outcomes. Using one of the vertical wells base case with one depletion case. Similarly, to the previous case the required information for hydraulic fracture simulation was sampled across the vertical well trajectories from the 3D mechanical earth model.

Fig.34 displays the base case before depletion which show that the frac is tending to grow up. Moreover, **Fig.35** show the fracture width, proppant coverage and conductivity in depletion case.

Some of the output from both Scenarios are as follow:

- Base Case Pclosure = 11,008 psi gives gradient of 0.79 psi/ft.
- Scenario-B Pclosure = 9,980 psi gives gradient of 0.72 psi/ft.

In the depletion case, the frac is contained since the depletion is applied in specific layer and it is obvious that the other layers acted as a pseudo barrier.

Table-3 shows the calculated results of the simulator which indicates the differences between the two cases such as the fracture length, conductivity which can visualized in the figures. Using different stresses to show the effect of stress changes effect in Hydraulic Fracturing in the same well. In the base case, the stress ranges from 11,000- 13,000 psi comparing with 10,000-12,000 psi for the depletion case.

Table 3 Hydraulic Fracturing 2nd Case Scenarios Results

Hydraulic Fracturing 2nd case Scenarios		Base Case Calculated Results	Depletion Case Calculated Results
Half Length	'Hydraulic' Length (ft)	337	458
	Propped length (ft)	312	444
PRESSURE:	Max Net Pressure (psi)	2846	4540
PROPPANT:	Average In Situ Conc.(lb/ft^2)	3.06	3.45
	Average Conductivity (md-ft)	6269	7316
	Fcd (KfW/k/Xf)	13.4	10.98
HEIGHT:	Max Fracture Height (ft)	244	163
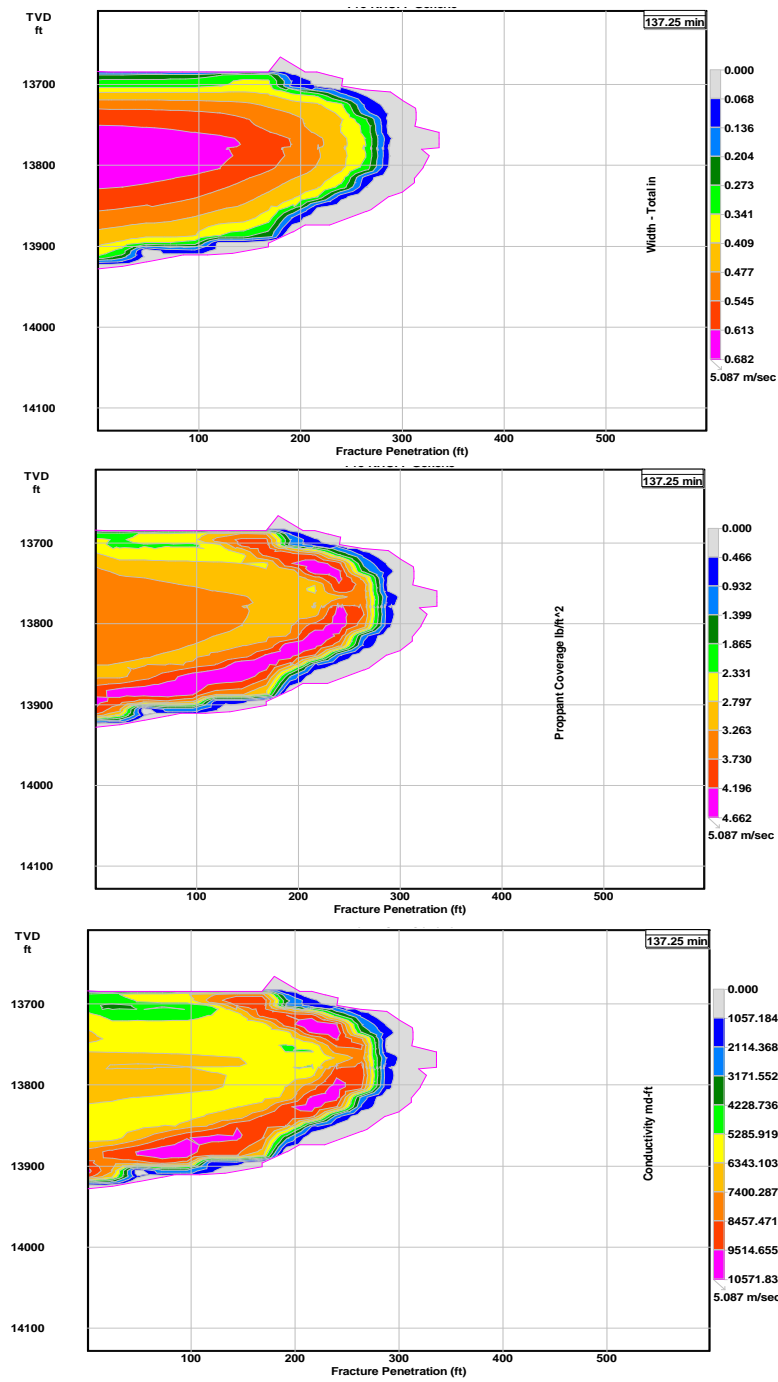
Figure 34   Hydraulic Fracturing 2nd Base Case (No Depletion)
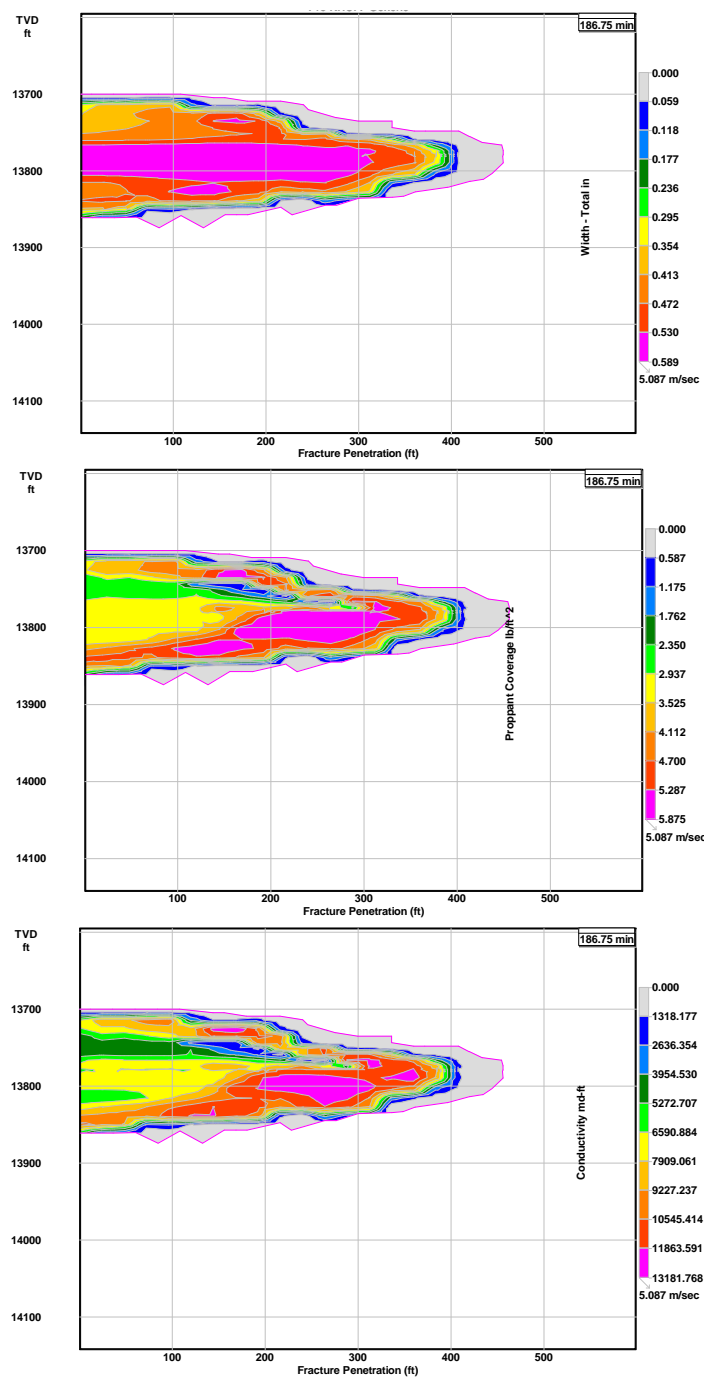
Figure 35   **Hydraulic Fracturing 2nd Depletion Case**

60

5.9 Wellbore Stability

Wellbore instability would occur after mechanical failure caused by in-situ stresses, erosion caused by fluid circulation or chemical caused by interaction of borehole fluid with the formation. Moreover, there are different types of associated issues that grouped as follows: hole closure or narrowing, hole enlargement or washouts, fracturing and collapse

Mud weight optimization is one of the most important factors in achieving best wellbore stability while drilling horizontal wells (also vertical). To maximize the drilled reservoir contact in the purpose of gas production enhancement from a tight Sandstone reservoir, horizontal drilling and multistage hydraulic fracturing methods have been implemented.

Maintaining wellbore stability has always been a challenge without enough geomechanical knowledge of the field. While drilling, several issues might be encountered in the drilling phase such as tight hole that needs excessive reaming, stuck pipe and complications while making trips. One of the most operational challenges during drilling a well specially the horizontal well is to drill with a single mud weight (MW) value which might lead to have drilling complications in depleted reservoir layers.

Wellbore stability modeling before drilling can help well design, aid determine a favorable wellbore trajectory and identify potential hazards. During drilling, wellbore stability models can be updated in real time as new information is received to reduce drilling uncertainty. Imaging logs from LWD tools can be used to determine breakout areas and drill induced fractures. Geomechanical analysis of rock strength allow complex wellbores to be successfully drilled.

5.10 Wellbore Stability Conceptual Case Study

Another conceptual case study was also conducted to understand the effect of depletion and subsequent stress changes in wellbore stability in the studied wells. One of the examples is illustrated in **Fig.36** &**37.**

Both Figures show the radial stress and collapse potential distribution around the wellbore. Both depletion scenarios were running at different depths and assuming same mud weight in the same wellbore and the results are shown in **Table-4**. Radial stress figures show a pattern in Depletion-1 while in Depletion-2 it shows random distribution.

Depletion-1 has the highest pore pressure and σ_{min} gradients, the radial stress in the far field is higher than Depletion-2 scenario. Depletion-2 appears to have high collapse potential in the min. stress direction around the wellbore but lower in the far-field. However, the potential to have breakouts around the wellbore in both scenarios are considerable.

Using same mud weight with applying different depletion scenario, Depletion-1 is showing smaller region of breakouts around the wellbore which is apparently more than Depletion-2. It is obvious that the breakouts tend to be in the minimum stress direction in both cases with different magnitude as the figure presents. Since Depletion-2 is in more depleted interval than Depletion-1, the potential of having collapse and losses is very high.
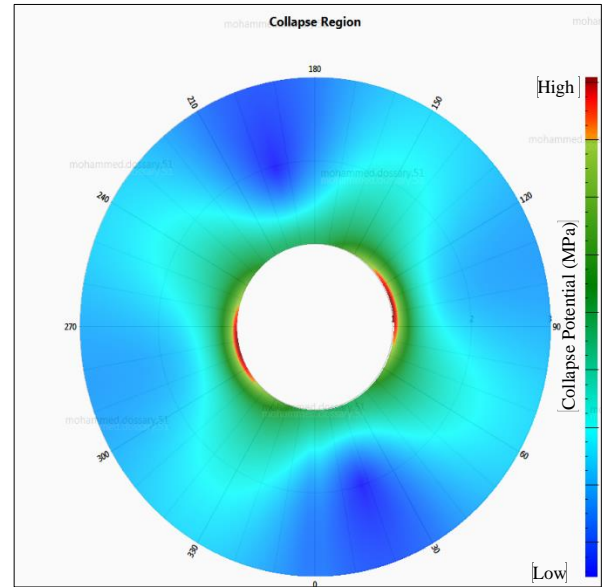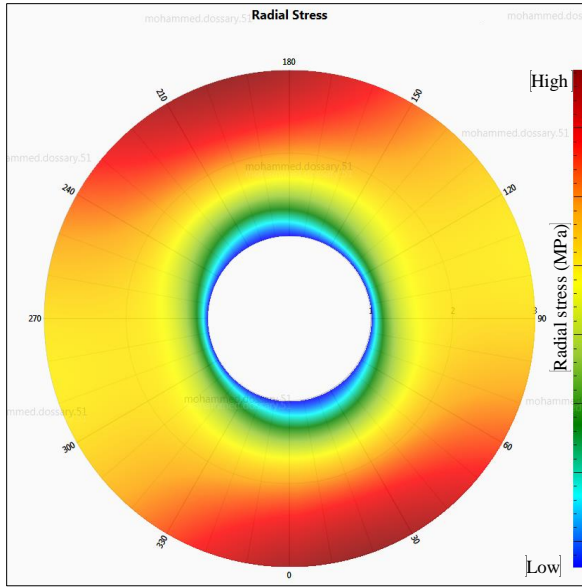
Figure 36   **Depletion-1 Effect Wellbore Stability Case Scenario**
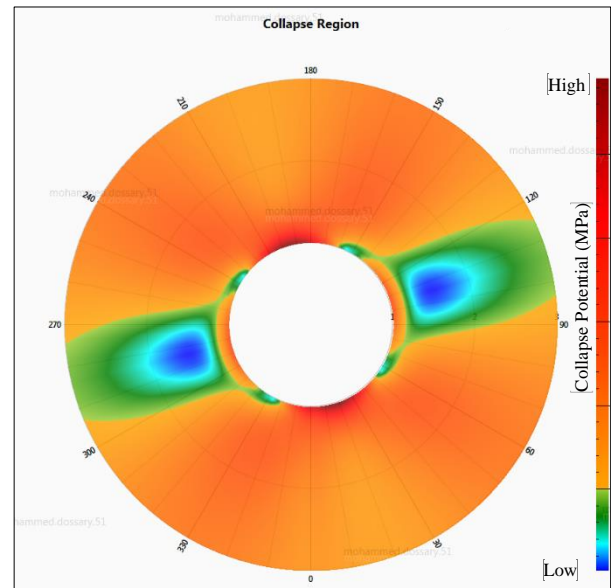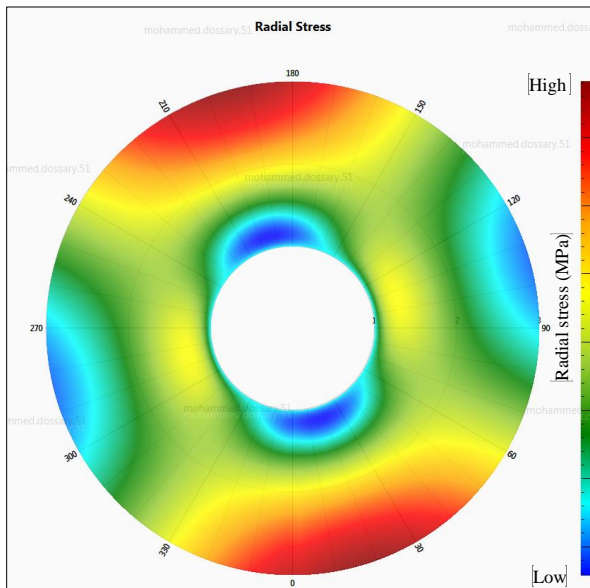
Figure 37   **Depletion-2 Effect Wellbore Stability Case Scenario**

Table 4 Wellbore Stability Cases Results

Scenario	Pore Pressure gradient, psi/ft	σ_{min} gradient, psi/ft
Depletion-1	0.32	0.62
Depletion-2	0.28	0.57

CHAPTER 6

CONCLUSIONS

Tight gas sandstone reservoirs that characterized by low permeability, low porosity, and having high elastic properties and rock strength considered as a challenging operational environment. Depletion effects add additional challenge to the drilling operation by moving the mud weight window to the right that can be mitigated by special mud design. On the other hand, depletion decreases the magnitude of the fracture gradient which makes the barriers between the reservoirs and adjust layers very distinct, that creates extra fracture containment, which would easier to predict the fracture heights as the hydraulic fractures play a decisive role in economy of these tight gas reservoirs since they enhance well productivity. Geomechanical modeling is a key driver in attaining optimum wellbore quality and providing a guideline to stimulation strategies.

A calibrated 1D geomechanical models have been constructed for the wells in the study area, the dynamic elastic, such as Young's modulus and Poisson's ratio and strength properties, such as compressive confining strength, friction angle and cohesion have calculated from acoustic and density logs and then converted to static properties and calibrated using available core data, overburden stress magnitude has been calculated by integrating available density logs, and the minimum horizontal stress magnitude has been modeled using poroelastic equation and then calibrated by available minifrac tests.

1D geomechanical properties have been upscaled and then extrapolated using sequential Gaussian simulation (SGS) to create 3D geomechanics properties. Final 3D geomechanical

models have been coupled with fluid flow using one-way coupling to investigate the impact of changing pore pressure into drilling and stimulation operations.

3D geomechanical models using simulation has been conducted to study the effects of depletion in complex tight gas formation in the study area. It is observed that the σH decreases in the depleted area but the adjoining layers experience higher σH. This change in stress increases the stress contrast between the layers.

Both hydraulic fracture conceptual cases show that higher stress can act as stress barrier and stop the propagation of hydraulic fractures and it will be contained.

Moreover, the stress contrast in adjoining layers due to depletion cannot be estimated using 1D Geomechanical models. Hence, a 3D geomechanical model is very helpful in designing hydraulic fractures in complex depleted tight gas reservoirs.

Wellbore stability cases have been constructed using different depletion scenarios. The wellbore collapse figures show that the breakouts occur in two different regions toward the minimum stress direction in both cases with different magnitudes. In conclusion, it is obvious that the breakouts tend to be in the minimum stress direction. Moreover, potential of having collapse and losses is very high in more depleted area.

REFERENCES

[1]   A. (Tony) Settari and Vikram Sen, "Geomechanics in Integrated Reservoir Modeling", OTC 19530, Offshore Technology Conference, 5 May 2008.

[2]   A. (Tony) Settari and Vikram Sen," The Role of Geomechanics In Integrated Reservoir Modeling", The Leading-Edge Article, May 2007.

[3]   Bradford, I.D.R., Fuller, J., Thompson, P.J., Walsgrove, T.R., 1998. "Benefits of Assessing the Solids Production Risk in a North Sea reservoir Using Elastoplastic modeling". SPE/ISRM Eurock '98 held in Trondheim, Norway, 8–10 July, 1998, pp. 261–269.

[4]   Chandong Chang, Mark D. Zoback, Abbas Khaksar, "Empirical Relations Between Rock Strength and Physical Properties in Sedimentary Rocks", Journal of Petroleum Science and Engineering 51 (2006) 223–237, 11 January 2006.

[5]   David Tran, Lloyd Buchanan and Long Nghiem, "Improved gridding technique for coupling geomechanics to reservoir flow", SPE 115514 , SPE Journal, 2010.

[6]   Dutta, "Geopressure Detection Reflection Seismic Data and Rock Physics Principles: Methodology and Case Histories from Deepwater Tertiary Clastics Basins", SPE 77820, SPE Asia Pacific Oil and Gas Conference and Exhibition, October 2002.

[7]   D. Moos, S. Willson and C.A. Barton, "Impact of Rock Properties on the Relationship Between Wellbore Breakout Width and Depth", Rock Mechanics Symposium, 27-31 May, Vancouver, Canada 2007.

[8]   Fjaer, E., Holt, R. M., Horsrud, P., Raaen, A. M. and Risnes, R. 2008: "Petroleum related rock mechanics, development in Petroleum science". 2nd Edition-Cambridge University Press.

[9]   Fjaer, E., Holt, R.M., Horsrud, P., Raaen, A.M., Risnes, R., "Petroleum Related Rock Mechanics". Elsevier, Amsterdam, 1992.

[10]   Freyburg, E., "Der Untere und mittlere Buntsandstein SWThuringen in seinen gesteinstechnicschen Eigenschaften". Ber. Dtsch. Ges. Geol. Wiss., A; Berlin 176, 911–919, 1972

[11]   Gang Han, Ben Vaughn, Andrew Davids, John Spokes, Robert Newman and Jose Adachi, "Development and Calibrations of a Coupled Reservoir Geomechanic

Model for Valhall Field", ARMA 13-163, The 47th US Rock Mechanics / Geomechanics Symposium held in San Francisco, June 2013.

[12]   Guilbot and Smith," Ekofisk 4D Seismic - Influence on Flow Simulation and Compaction Modeling", OTC 14149, 2002 Offshore Technology Conference, May 2002.

[13]   Herwanger, J. and Koutsabeloulis N. 2011: "Seismic Geomechanics". How to build and calibrate geomechanical models using 3D and 4D seismic data, EAGE, The Netherlands.

[14]   K. Qui, J.R. Marsden, Y. Solovyov, M. Safdar, and O. Chardac and M. Shatwan, "Downscaling Geomechanics Data for Thin Beds Using Petrophysical Techniques", SPE 93605, 14th SPE Middle East Oil and Gas Show and Conference, 12 March 2005.

[15]   Kabini Qui, Ning Cheng, Xiangui Ke, Yang Liu, Lirong Wang, Yong Wang and Pi Xiong, "3D Reservoir Geomechanics Workflow and Its Applications to a Tight Gas Reservoir in Westren China", IPTC 17115, International Petroleum Technology Conference, 26 March 2013.

[16]   Khazanehdari and Dutta, "High-resolution pore pressure prediction using seismic inversion and velocity analysis", SEG, New Orleans Annual Meeting, 2006.

[17]   Koster et al., "Reservoir monitoring of the Draugen field through time-lapse seismic and it's business impact", SPE 87300, 9th Abu Dhabi International Petroleum Exhibition and Conference, October 2000.

[18]   Koutsabeloulis, N. C., and S. A. Hope, 1998. "Coupled Stress / Fluid / Thermal Multi-Phase Reservoir Simulation Studies Incorporating Rock Mechanics", Proc. SPE/ISRM Rock Mechanics In Petroleum Engineering Conference, 2: 449-454.

[19]   Maurice B. Dusseault, "Geomechanical Challenges in Petroleum Reservoir Exploitation", KSCE 12205, KSCE Journal of Civil Engineering, 2011.

[20]   McNally, G.H., "Estimation of coal measures rock strength using sonic and neutron logs". Geoexploration 24, 381–395, 1987.

[21]   Moos, D., Zoback, M.D., Bailey, L., 1999. "Feasibility study of the stability of openhole multilaterals, Cook Inlet", Alaska. 1999 SPE Mid-Continent Operations Symposium held in Oklahoma City, Oklahoma, 28–31 March 1999, SPE 52186.

[22]   M.R. Jalali and M.B. Dusseault, "Coupled Fluid-Flow and Geomechanics In Naturally Fractured Reservoirs", 5th Asian Rock Mechanics Symposium, 28 November 2008

[23]   Osman Hamid and Zillur Rahim, "Mechanical Properties of Carbonate Formation and Their Influences on Drilling and Hydraulic Fracture Modeling", SPE 172573, SPE Middle East Oil & Gas Show and Conference, 8 March 2015.

[24]   Osman Hamid, Haytham Osman and Sarah Alamer "Enhanced Assessment of Stress Dependent Permeability of Sandstone Rock", SPE 192605, Abu Dhabi International Petroleum and Conference, 2018.

[25]   Osman Hamid, "Geomechanical Characterization of Hydraulic Fracture in Tight Carbonates due to Depletion", SPE 172797, 19th Middle East Oil & Gas Show and Conference held in Bahrain International Exhibition & Convention Centre, 9 March 2015.

[26]   P.J. Hatchell*, A. van den Beukel, M.M. Molenaar, K.P. Maron, and C.J. Kenter, Rijswijk; and J.G.F. Stammeijer, J.J. van der Velde, and C.M. Sayers, "Whole earth 4D: reservoir monitoring geomechanics",2002.

[27]   P. Longuemare, M. Mainguy, P. Lemonnier, A. Onaisi, Ch. Gerard and N. Koutstabeloulis, "Geomechanics in Reservoir Simulation: Overview of Coupling Methods and Field Case Study ", Oil & Gas Science and Technology, 2002.

[28]   R.O. Lindsay and D.W. Ratcliff, Diamond, "Pore Pressure Prediction From 3-D Seismics", OTC 8337, Offshore Technology Conference, 8 May1997.

[29]   Sayers et al., "Pore Pressure Prediction for the Cocuite Field, Veracruz Basin", SPE 77360, SPE Annual Technical Conference and Exhibition, October 2002.

[30]   Sirat, M., Al-Arfi, S., Al-Shaarawi, A., Ahmed M., Zhang, X., Ghorayeb, K., and Daniels, J., 2013. "Implication and Uncertainty of 1D Mechanical Earth Model for Hydraulic Fracturing in a Carbonate Gas Reservoir in Abu Dhabi", ADIPEC 2013, Abu Dhabi, UAE.

[31]   Settari and Mourits, "A Coupled Reservoir and Geomechanical Simulation System", SPE 50939, SPE Journal, 1998.

[32]   Sone Hiroki. 2012: "Mechanical properties of shale gas reservoir rocks and its relationship to the in-situ stress variation observed in shale gas reservoir". PhD thesis Stanford University SRB volume 128.

[33]   Thomas Berad and Romain Prioal, "Mechanical Earth Model", Schlumberger, oilfield review, 2016.

[34]   Vernik, L., Bruno, M., Bovberg, C., "Empirical relations between compressive strength and porosity of siliciclastic rocks". Int. J. Rock Mech. Min. Sci. Geomech. Abstr. 30, 677–680., 1993

[35]   W. Yuezhi, L. Zijun and H. Lixin, "Model and Calculation of In Situ Stresses in Anisotropic Formations", PETSOC-97-117, 48th Annual Technical Meeting of The Petroleum Society, 8 June 1997.

Vitae

Name   :Mohammed Jaber Al-Dossary

Nationality   :Saudi

Date of Birth   :9/27/1988

Email   :dossmj779@gmail.com

Address   :34265-7270 Shula District, Dammam

Academic Background

Graduated in 2011 with a bachelor's degree of Petroleum Engineering

Publication

Accepted in the 11th IPTC to be held on March 2019 in China, Paper#: IPTC-19097